

Original Article

Cite this article: Hu F, Huang W, Yang Z, Wilde SA, Furnes H, Luo M, and Zhang K (2020) Geochemistry and zircon U–Pb–Hf isotopes of the Mante Aobao granite porphyry at East Ujimqin Banner, Inner Mongolia: implications for petrogenesis and tectonic setting. *Geological Magazine* **157**: 1068–1086. <https://doi.org/10.1017/S0016756819001274>

Received: 17 May 2019

Revised: 20 September 2019

Accepted: 24 September 2019

First published online: 18 November 2019


Keywords:

Zircon U–Pb dating; geochemistry; I-type granite; Late Ordovician; subduction of Paleo-Asian Ocean

Author for correspondence:

Kexin Zhang, Email: kx_zhang@cug.edu.cn

Geochemistry and zircon U–Pb–Hf isotopes of the Mante Aobao granite porphyry at East Ujimqin Banner, Inner Mongolia: implications for petrogenesis and tectonic setting

Fei Hu¹ , Wei Huang², Zeli Yang³, Simon A. Wilde⁴, Harald Furnes⁵, Mansheng Luo⁶ and Kexin Zhang¹ 

¹Institute of Geological Survey, China University of Geosciences, Wuhan 430074, China; ²Guangdong Geologic Survey Institute, Guangzhou 510110, China; ³Tianjin Center of China Geological Survey, Tianjin 300170, China; ⁴School of Earth and Planetary Sciences, Curtin University, PO Box U1987, WA 6845, Perth, Australia; ⁵Department of Earth Science, University of Bergen, Bergen 5173, Norway and ⁶State Key Laboratory of Biogeology and Environmental Geology, China University of Geosciences, Wuhan 430074, China

Abstract

We present detailed petrography, geochemistry and zircon U–Pb–Hf isotopes of the Mante Aobao granite porphyry in East Ujimqin Banner, Inner Mongolia, with the aim of determining its age and petrogenesis, important for understanding the early Palaeozoic tectonic evolution of the Xing'an–Mongolian Orogenic Belt. The Mante Aobao granite porphyry consists of plagioclase, quartz and minor biotite, but without amphibole. Zircon U–Pb analyses yield ages of 450 ± 1 Ma and 445 ± 2 Ma for the granite porphyry, indicating that it formed during Late Ordovician time. The granite porphyry is metaluminous to slightly peraluminous (aluminous saturation index $A/CNK = 0.98–1.11$) with high SiO_2 , K_2O and Na_2O concentrations and differentiation index ($DI = 85–90$). Chondrite-normalized rare earth element (REE) patterns display enrichment of light REEs (LREEs) with high ratios of $(\text{La}/\text{Yb})_N$ and negative Eu anomalies. In the mantle-normalized multi-element variation diagrams, all samples are characterized by depletions of high-field-strength elements (HFSEs; Nb, Ta and Ti) and enrichments of large-ion lithophiles (LILEs; Rb, Th, U and K). These geochemical features indicate that the granite porphyry is a highly fractionated I-type granite and formed in a subduction-related setting. Zircon grains have positive $\epsilon_{\text{Hf}}(t)$ values of $+9.2$ to $+11.2$, and $T_{\text{DM2}}(\text{Hf})$ ages of 691–821 Ma, suggesting that the granite porphyry was generated by partial melting of Neoproterozoic juvenile crust with involvement of fractional crystallization during magmatic evolution. It is likely that underplating of mantle-derived magmas during Late Ordovician time provided the necessary heat to partially melt this juvenile crust. Combined with the regional geological data, we infer that the Mante Aobao granite porphyry was emplaced in an active continental margin setting that was probably related to the northwards subduction of the Paleo-Asian Plate beneath the South Mongolian Terrane along the Sonid Zuqi–Xilinhot axis.

1. Introduction

The Xing'an–Mongolian Orogenic Belt is located between the Siberian and North China cratons (Fig. 1a), and belongs to the central-eastern segment of the Central Asian Orogenic Belt (CAOB), which is one of the largest Phanerozoic accretionary orogenic belts and the most important site of Phanerozoic crustal growth on Earth (Sengör & Natal'in, 1996; Jahn *et al.* 2000; Kovalenko *et al.* 2004; Windley *et al.* 2007; Li *et al.* 2014a). Since *c.* 1.0 Ga, the precursor to the Central Asian Orogenic Belt, the Paleo-Asian Ocean, underwent multiple subduction, accretion of island arcs and obduction of ophiolites before terminal collision between the North China and Siberian cratons at *c.* 250 Ma (Jahn *et al.* 2004; Guo *et al.* 2009; Li *et al.* 2014b). The evolution of the central part of the Paleo-Asian Ocean was closely related to the formation of the Xing'an–Mongolian Orogenic Belt (Tang, 1990, 1992; Xu & Chen, 1997; Xiao *et al.* 2003; Chen *et al.* 2012; Xu *et al.* 2013; Shi *et al.* 2013; Zhang *et al.* 2013, 2015b; Li *et al.* 2011, 2014c). Previous studies show that the Paleo-Asian Ocean underwent a bi-directional subduction process after late Proterozoic time, resulting in the formation of the Xing'an–Mongolian Orogenic Belt (Xiao *et al.* 2003). Numerous studies have emphasized the role of multiple subduction in the final closure of the Paleo-Asian Ocean and it is widely accepted that this collision gave rise to the Solonker Suture Zone (Wang & Fan, 1997; Li *et al.* 2007; Jian *et al.* 2008; Tong *et al.* 2010; Wang *et al.* 2013), but controversy remains about the timing and mechanisms involved. For instance, Tang & Shao (1996) suggested, based on a study of the Ondor Sum ophiolites, that subduction of the Paleo-Asian Ocean began during

Cambrian–Ordovician time and terminated during Devonian – Early Carboniferous time. Xiao *et al.* (2003) considered that the Paleo-Asian Ocean underwent bi-directional subduction during the Cambrian–Silurian periods, but that subduction halted before Devonian – Early Carboniferous time, before recommencing after the Late Carboniferous Period. It has been suggested by many authors utilizing palaeogeographic, geochronological and geochemical data from central Inner Mongolia that subduction started during the Ordovician Period and ended during the late Permian Period (Jong *et al.* 2006; Li, 2006; Chen *et al.* 2009; Zhang *et al.* 2009; Wu *et al.* 2011; Wilde, 2015; Wilde & Zhou, 2015; Ma *et al.* 2019; Xu *et al.* 2019). Moreover, most geologists considered that the early bi-directional subduction of the Paleo-Asian Ocean led to the formation of the Bainaimiao and Baiyinbaoli island arcs, with the final collision along the Solonker Suture Zone (Xiao *et al.* 2003; Chen *et al.* 2009). Li *et al.* (2014c) proposed that there was long-lasting bi-direction subduction of the Paleo-Asian Ocean crust from early Palaeozoic to middle Permian time, based on the north Baiyinbaoli island arcs and the south Ondor Sum subduction–accretion complex in the Solonker Suture Zone. Jian *et al.* (2010b) and Shi *et al.* (2014, 2016) considered that the Paleo-Asian Ocean mainly experienced the following events: Ordovician bi-directional subduction, Silurian accretion, Devonian extension, Permian subduction to the south with extension to the north, and continent–continent collision during the late Palaeozoic – early Mesozoic eras.

According to previous studies, the Xing'an–Mongolian Orogenic Belt in NE China formed as a result of subduction and accretion during early Palaeozoic time (Fig. 1a; Chen & Xu, 1996; Chen *et al.* 2000; Liu *et al.* 2003; Xiao *et al.* 2003; Tao *et al.* 2005; Xu, 2005; Zhao *et al.* 2012; Xu *et al.* 2013, 2014; Li *et al.* 2016). Nevertheless, early Palaeozoic magmatic events are poorly documented in the Uliastai continental margin of the north-central Xing'an–Mongolian Orogenic Belt (Fig. 1b); it is unclear at present whether this reflects the true distribution or is a consequence of insufficient geochronological data hampering our understanding of the subduction history of the Paleo-Asian Ocean and the development of the Xing'an–Mongolian Orogenic Belt. Here we present new zircon U–Pb–Hf isotopes and whole-rock major and trace-element compositions of the Mante Aobao granite porphyry in the East Ujimqin Banner area of the central Xing'an–Mongolian Orogenic Belt (Fig. 1b, c), and evaluate its petrogenesis and tectonic setting.

2. Geological setting

2.a. Regional geology

The Xing'an–Mongolian Orogenic Belt in Inner Mongolia is located in the central-eastern segment of the Central Asian Orogenic Belt (Fig. 1a). It is an ENE-trending tectonic collage composed of the remnants of ophiolites, arcs, accretionary wedges and associated volcano-sedimentary rocks. From north to south, the Xing'an–Mongolian Orogenic Belt is divisible into six tectonic units (Fig. 1b): the Uliastai continental margin; the Hegenshan ophiolite arc-accretion complex; the Baolidao arc-accretion complex; the Solonker Suture Zone; the Ondor Sum subduction–accretion complex; and the Bainaimiao island arc (Xiao *et al.* 2003).

The Uliastai continental margin extends along the China–Mongolia border and connects with the Nuhetdavaa terrane to the west (Badarch *et al.* 2002; Zhou *et al.* 2017; Fig. 1b). The strata exposed in the Uliastai continental margin are Ordovician,

Silurian, Devonian, Carboniferous – lower Permian, Jurassic and Cretaceous volcano-sedimentary rocks and Tertiary and Quaternary sediments (Tang & Zhang, 1991; Su, 1996; Xin *et al.* 2011). Palaeozoic magmatism is extensive and upper Carboniferous – lower Permian intrusive rocks are widespread, dominated by potassium calc-alkali and alkali granites (Zhang, 2008; Yang, 2016, 2017). Recently, several lower Palaeozoic arc-related magmatic complexes have been recognized (Fig. 1b), including the Wulagai gabbroic diorites (Yang *et al.* 2018), the gabbros in the western sector of the Shamai area (Yang, 2016), the Chaobuleng gabbros (Li *et al.* 2016), the Gilgalantu complex plutons (Yang, 2016; Yang *et al.* 2017), the granodiorite in the western sector of the Mandubaolige area (Yang, 2016) and the Geri Obo granites (Zhao *et al.* 2012). The Hegenshan ophiolite arc-accretion complex extends NE for c. 500 km to the north of the Erenhot–Hegenshan Fault (Xiao *et al.* 2003; Zhang *et al.* 2015a, b), and contains abundant ophiolitic blocks with various ages. The largest blocks are the lower Carboniferous arc-related supra-subduction zone (SSZ)-type ophiolite at Hegenshan (Robinson *et al.* 1999; Jian *et al.* 2012) and several tectonic blocks at Erenhot (Zhang *et al.* 2015a, b). The Baolidao arc-accretion complex contains abundant lower Carboniferous ophiolites (Miao *et al.* 2007), blueschists (Xu *et al.* 2013) and upper Carboniferous magmatic arc rocks (Chen *et al.* 2000, 2009), which were intruded by lower Permian alkaline and peralkaline granites (Shi *et al.* 2004).

The Solonker Suture Zone formed during the end of the Palaeozoic Era and represents the collision zone between the Siberian and North China cratons (Xiao *et al.* 2003). It extends from Solonker, via Sonid Zuoqi and Xilinhot of Inner Mongolia, and further east to NE China (Fig. 1b). There are two regional faults representing Palaeo-suture zones: the Solonker–Xar Moron Fault and the Linxi Fault. The Solonker–Xar Moron Fault marks the southern boundary of the suture zone, and the Linxi Fault marks the northern boundary (Xiao *et al.* 2003). The Ondor Sum subduction–accretion complex mainly comprises lower Palaeozoic blueschists (Tang & Yan, 2007) and a series of ophiolite blocks of Palaeozoic age (Wang & Liu, 1986; Xiao *et al.* 2003; Li, 2006; Miao *et al.* 2007; Zhou *et al.* 2017). During late Palaeozoic subduction that was accompanied by the intrusion of several plutons, the Carboniferous and Permian volcano-sedimentary sequences were accreted onto the active margin of the North China Craton. The Bainaimiao island arc is located north of the Chifeng–Bayan Obo Fault. It comprises Middle Ordovician – lower Silurian volcano-sedimentary sequences and magmatic arcs (Jian *et al.* 2008; Zhang *et al.* 2013).

2.b. The study area, samples and petrography

The study area is located about 60 km NE of the East Ujimqin Banner area and lies in the Uliastai continental margin zone (Fig. 1b). Lithostratigraphic units mapped in the study area are shown in Figure 1c. The Lower Ordovician Tongshan Formation (O_{1t}) is composed of dark brown siltstone, whereas the Lower–Middle Ordovician Duobaoshan Formation (O_{1–2d}) is composed of calc-alkali andesite, rhyolite, spilite-keratophyre, tuff and interbedded tuffaceous sandstone. The upper Carboniferous – lower Permian Baoligaomiao Formation ((C₂–P₁)bl) comprises volcanic breccia, rhyolite and dacite. The lower Cretaceous Baiyingaolao Formation (K_{1b}) is composed of acidic volcanic rocks, whereas the Pliocene Baogedawula Formation (N_{2b}) consists of brick-red clays.

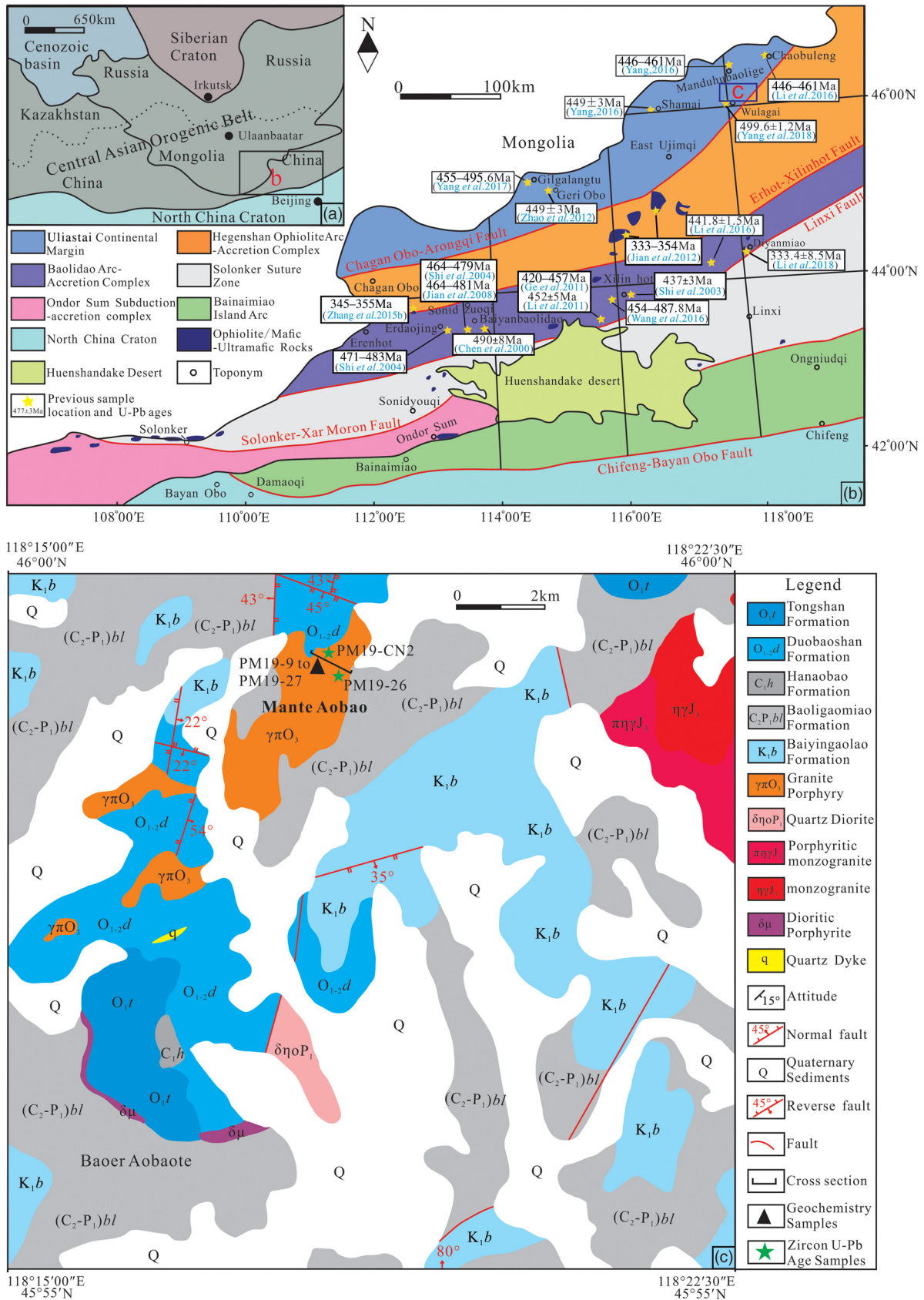


Fig. 1. (Colour online) Geological sketch maps showing the location and tectonic setting of the study area: (a) Central Asian Orogenic Belt (modified from Jian et al. 2008 and Wu et al. 2015a); (b) central and eastern Inner Mongolia, showing distribution of the lower Palaeozoic intrusive rocks (modified from Xiao et al. 2003 and Li et al. 2016); and (c) the relationship of the Mante Aobao granite porphyry to rock units in the East Ujimqin Banner area, Inner Mongolia.

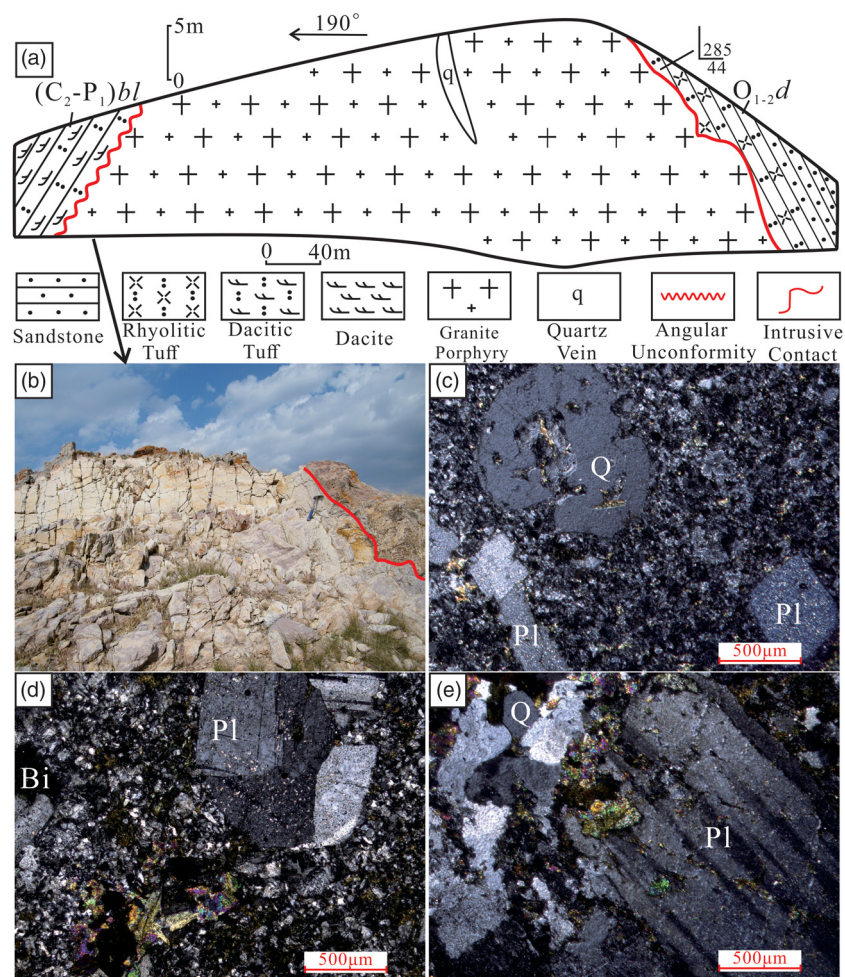


Fig. 2. (Colour online) (a) Sketch and (b) field photograph of contact relationships between the granite porphyry and the Duobaoshan Formation ((C₂-P₁)bl) and Baoligaomiao Formation (O_{1-2d}); and (c-e) cross-polarized photomicrographs of the granite porphyry. Bi - biotite; Pl - plagioclase; Q - quartz.

Regional geological surveys have revealed the presence of four NE-SW-trending, lower Palaeozoic plutons that have a total area of c. 6.5 km² (Fig. 1c), one of which is the Mante Aobao pluton. The Mante Aobao pluton was named after the Mante Aobao area, which lies c. 60 km NE of the East Ujimqin Banner area. In the field, the Mante Aobao pluton is granitic throughout and mainly consists of fine- to medium- grained granite porphyry devoid of any mafic-ultramafic intrusions or mafic enclaves (Fig. 1c). Chilled margins or flow structures have not been observed in the pluton, and it is undeformed. Field relationships show that the granite porphyry was emplaced into sandstone, limestone and volcanic rocks of the Duobaoshan Formation, and is unconformably overlain by volcanic rocks of the Baoligaomiao Formation (Figs 1c, 2a, b). We collected two samples for zircon U-Pb-Hf isotope analysis (PM19-26, 118° 17' 47.626" E, 45° 58' 44.961" N; PM19-CN2, 118° 17' 37" E, 45° 58' 57" N; Fig. 1c) and 11 samples for geochemical analyses (PM19-9 to PM19-27). The location of the samples is highlighted on Figure 1c. In order to avoid the influence of alteration, the freshest rocks were collected for geochemical analyses.

The granite porphyry has a porphyritic texture and a massive structure (Fig. 2c-e). Phenocryst minerals are plagioclase (15%), quartz (10%) and minor biotite (5%). The plagioclase is tabular and 0.3–2.5 mm across, and some of the plagioclase is altered to sericite and clay minerals. The quartz is anhedral and is 0.3–2.0 mm across, whereas the biotite forms dark laths that are

0.3–1.0 mm in length and unevenly distributed throughout the rock. The phenocrysts are set in a matrix of felsic minerals and biotite (c. 70%). The accessory minerals are magnetite, titanite, apatite and zircon.

3. Analytical methods

3.a. Zircon U-Pb analysis

As noted above, two granite porphyry samples were collected for zircon U-Pb and Lu-Hf isotopic analysis. Zircons were separated following standard procedures involving crushing and heavy liquid and magnetic techniques, and were handpicked under a binocular microscope. Zircons were then mounted in epoxy resin and the grain mount was abraded and polished in order to cut the crystals in half for analysis. In order to characterize the internal structures of the zircons, transmitted and reflected light photomicrographs and cathodoluminescence (CL) images were obtained and used to select the sites for U-Th-Pb analyses. CL images were obtained using a JXA-8800R electron microprobe at the Tianjin Institute of Geology and Mineral Resources (TIGMR), Tianjin. U-Pb analyses were conducted on a Thermo Scientific Neptune multicollector inductively coupled plasma mass spectrometer (MC-ICP-MS) coupled with a 193 nm laser ablation system at TIGMR. Data acquisition for each analysis took 20 s for the background and 40 s for the signal. Mass discrimination in the mass spectrometer

and elemental fractionation were corrected by calibration against the homogeneous zircon standards 91500 and GJ-1; the detailed instrument operating conditions were described by Liu *et al.* (2008). All zircon data were acquired at a spot size of 32 μm . Off-line selection and integration of background and analytical signals, time-drift corrections and quantitative calibrations for trace-element analyses and U–Pb dating were performed using ICPMSDataCal version 9.0 software (Liu *et al.* 2010). The common lead correction was calculated using the Excel software ComPbCorr#3_15G (Andersen, 2002). Concordia diagrams were prepared and weighted mean calculations were performed using Isoplot/Ex_ver3 (Ludwig, 2003). All ages are quoted at the 2σ level of uncertainty.

3.b. Zircon Lu–Hf isotopic analysis

Zircon Hf isotope measurements were performed on the dated zircons using a Neptune Plus MC-ICP-MS (Thermo Fisher Scientific, Germany) in combination with a Geolas 2005 excimer argon fluoride (ArF) laser ablation system (Lambda Physik, Göttingen, Germany), hosted at the State Key Laboratory of Geological Processes and Mineral Resources, China University of Geosciences, Wuhan. The analyses were conducted on either the same sites previously analysed for U–Pb dating or on adjacent areas, guided by the CL images. All data were acquired with a spot size of 44 μm . Each measurement comprised 20 s of background acquisition followed by 50 s of ablation signal acquisition. The detailed operating conditions for the laser ablation system, the specific MC-ICP-MS instrument and the analytical methods involved were presented in Hu *et al.* (2012). The $^{179}\text{Hf}/^{177}\text{Hf}$ and $^{173}\text{Yb}/^{171}\text{Yb}$ ratios were used to calculate the mass bias of Hf (β_{Hf}) and Yb (β_{Yb}), which were normalized to $^{179}\text{Hf}/^{177}\text{Hf} = 0.7325$ and $^{173}\text{Yb}/^{171}\text{Yb} = 1.132685$ (Fisher *et al.* 2014) using an exponential correction for mass bias. Interference of ^{176}Yb on ^{176}Hf was corrected by measuring the interference-free ^{173}Yb isotope and using $^{176}\text{Yb}/^{173}\text{Yb} = 0.79639$ (Fisher *et al.* 2014) to calculate $^{176}\text{Yb}/^{177}\text{Hf}$. Similarly, the relatively minor interference of ^{176}Lu on ^{176}Hf was corrected by measuring the intensity of the interference-free ^{175}Lu isotope and using the recommended $^{176}\text{Lu}/^{175}\text{Lu} = 0.02656$ (Blichert-Toft & Albarede, 1997) to calculate $^{176}\text{Lu}/^{177}\text{Hf}$. We used the mass bias of Yb (β_{Yb}) to calculate the mass fractionation of Lu because of their similar physicochemical properties. The offline selection and integration of analytical signals, as well as the mass bias calibrations, were performed using ICPMSDataCal software (Liu *et al.* 2010). The decay constant for ^{176}Lu and the chondritic ratios of $^{176}\text{Hf}/^{177}\text{Hf}$ and $^{176}\text{Lu}/^{177}\text{Hf}$ used in the calculations were $1.865 \times 10^{-11} \text{ a}^{-1}$ (Scherer *et al.* 2001), and 0.282772 and 0.0332 (Blichert-Toft & Albarede, 1997), respectively. The single-stage model age (T_{DM1}) was calculated relative to the depleted mantle with a present-day $^{176}\text{Hf}/^{177}\text{Hf}$ ratio of 0.28325 and a $^{176}\text{Lu}/^{177}\text{Hf}$ ratio of 0.0384 (Griffin *et al.* 2000); two-stage model ages (T_{DM2}) were calculated by assuming a mean $^{176}\text{Lu}/^{177}\text{Hf}$ value of 0.015 for the average continental crust (Griffin *et al.* 2000). Initial $^{176}\text{Hf}/^{177}\text{Hf}$ ratios and $\epsilon_{\text{Hf}}(t)$ values were calculated using the mean zircon crystallization ages of the samples, as determined by the U–Pb dating.

3.c. Whole-rock major and trace-element analysis

Eleven homogeneous granite porphyry samples were selected from the least weathered and altered outcrops. Fresh, homogeneous samples were pulverized using an agate ring mill to <200 mesh. The major elements were analysed using X-ray fluorescence

spectrometry (3080E1; Rigaku, Tokyo, Japan) and plasma spectrometry at the Hubei Geological Research Laboratory. FeO was obtained by titrating with potassium dichromate solution in the Hubei Geological Research Laboratory, with analytical uncertainty <5%. Trace-element aliquots were digested in HF + HNO₃ in Teflon bombs and analysed with an Agilent 7500a ICP-MS at the Hubei Geological Research Laboratory following the protocols of Liu *et al.* (2008), with an analytical uncertainty of <1–3%.

4. Analytical results

4.a. Zircon U–Pb ages

Zircon LA-ICP-MS U–Pb dating results are listed in Table 1. Zircon grains from the two granite porphyry samples were mostly colourless, columnar crystals (60–200 μm long) with length:width ratios of 1.2:1 to 3:1. In CL images (Fig. 3c), most of the zircons show strong oscillatory zoning, typical of magmatic crystallization (Corfu *et al.* 2003; Wu & Zheng, 2004), but some zircons are dark in CL and lack zoning (Fig. 3c). The content of radiogenic Pb was 7–43 ppm, with little variation. The Th/U ratio ranged from 0.36 to 1.08, values characteristic of magmatic zircons. The zircon crystallization ages of the samples were <1000 Ma, so the $^{206}\text{Pb}/^{238}\text{U}$ age was adopted.

A total of 24 spots were analysed on zircons from sample PM19-26; of these, 17 were concordant, recording a weighted mean $^{206}\text{Pb}/^{238}\text{U}$ age of 450 ± 1 Ma (mean square weighted deviation or MSDW = 0.61) (Fig. 3a). One analysis (26-2) recorded an older $^{206}\text{Pb}/^{238}\text{U}$ age of 472 ± 3 Ma, which was interpreted as a xenocryst. Six analyses were strongly discordant (Fig. 3a) and were not used in the age calculation. The reason for this is unclear, but perhaps represents an incorrect ^{204}Pb correction.

A total of 32 sites were analysed on zircons from sample PM19-CN2, and 21 sites were concordant and recorded a weighted mean $^{206}\text{Pb}/^{238}\text{U}$ age of 445 ± 2 Ma (MSDW = 0.89) (Fig. 3b). The remaining 11 analyses gave younger and discordant ages. These zircons mostly have CL-dark features and some lack typical growth zoning (Fig. 3c), indicating that they may have undergone a degree of metamictization causing Pb loss (Wan *et al.* 2011).

4.b. Zircon Lu–Hf isotope data

The sites used for U–Pb dating were also used for *in situ* zircon Hf isotope analysis (Table 2; Fig. 3c). Eight analyses of the c. 450 Ma zircons from granite porphyry sample PM19-26 yielded $^{176}\text{Hf}/^{177}\text{Hf} = 0.282767$ – 0.282818 , with $\epsilon_{\text{Hf}}(t)$ values ranging from +9.2 to +10.8 and $T_{\text{DM2}} = 719$ – 821 Ma. Eight analyses of the c. 445 Ma zircons from granite porphyry sample PM19-CN2 yielded $^{176}\text{Hf}/^{177}\text{Hf} = 0.282776$ – 0.282828 , with $\epsilon_{\text{Hf}}(t)$ values ranging from +9.3 to +11.2 and $T_{\text{DM2}} = 691$ – 810 Ma. In the $\epsilon_{\text{Hf}}(t)$ versus age diagram (Fig. 4a, b), nearly all of the samples plot in the field of igneous rocks from the Eastern CAO (Xiao *et al.* 2004; Chen *et al.* 2009), but are distinct from those of the Yanshan Fold and Thrust Belt (YFTB), as determined by Yang *et al.* (2006).

4.c. Major and trace elements

A complete dataset of whole-rock major- and trace-element analyses of 11 representative samples from the Mante Aobao granite porphyry is presented in Table 3. All the samples display high SiO₂ values, with a narrow range from 71.69 to 72.33 wt%, with high Na₂O values (3.61–5.01 wt%) and moderate K₂O values

Table 1. LA-ICP-MS zircon U–Pb dating results for the Mante Aobao granite porphyry in East Ujimqin Banner, Inner Mongolia. All U–Pb zircon ages are corrected for ²⁰⁴Pb using Excel software ComPbCorr#3_15G (Andersen, 2002)

Sample no.	Content (ppm)				Ratio						Age (Ma)				Concordance (%)		
	²³² Th/ ²³⁸ U	Pb	Th	U	²⁰⁶ Pb/ ²³⁸ U	1σ	²⁰⁷ Pb/ ²³⁵ U	1σ	²⁰⁷ Pb/ ²⁰⁶ Pb	1σ	²⁰⁶ Pb/ ²³⁸ U	1σ	²⁰⁷ Pb/ ²³⁵ U	1σ		²⁰⁷ Pb/ ²⁰⁶ Pb	1σ
Sample PM19-26, granite porphyry, 45° 58' 44.961" N, 118° 17' 47.626" E																	
PM19-26-1	0.570	11	86	151	0.0725	0.0004	0.5602	0.0192	0.0561	0.0019	451	3	452	16	455	75	100
PM19-26-2	0.446	7	43	97	0.0760	0.0004	0.5911	0.0154	0.0564	0.0013	472	3	472	12	469	53	100
PM19-26-3	0.445	15	93	210	0.0723	0.0005	0.5642	0.0151	0.0566	0.0011	450	3	454	12	476	43	99
PM19-26-4	0.40	8	33	83	0.0800	0.0005	1.2885	0.0334	0.1168	0.0028	496	3	841	22	1907	43	30
PM19-26-5	0.635	14	119	188	0.0716	0.0004	0.5656	0.0091	0.0573	0.0008	446	3	455	7	503	32	98
PM19-26-6	0.479	11	71	148	0.0722	0.0004	0.5529	0.0127	0.0555	0.0012	450	3	447	10	433	49	99
PM19-26-7	0.836	33	342	409	0.0723	0.0004	0.5554	0.0105	0.0557	0.0010	450	3	449	8	440	41	100
PM19-26-8	0.384	9	48	124	0.0721	0.0004	0.5555	0.0110	0.0559	0.0011	449	3	449	9	447	43	100
PM19-26-9	0.459	17	105	229	0.0724	0.0004	0.5575	0.0097	0.0559	0.0009	450	3	450	8	448	36	100
PM19-26-10	0.387	8	43	110	0.0723	0.0004	0.5549	0.0133	0.0557	0.0013	450	3	448	11	439	52	100
PM19-26-11	0.492	12	79	160	0.0725	0.0007	0.8402	0.0431	0.0841	0.0032	451	4	619	32	1295	75	63
PM19-26-12	0.504	8	57	114	0.0720	0.0006	0.5609	0.0236	0.0565	0.0020	448	4	452	19	473	80	99
PM19-26-13	0.407	8	44	107	0.0717	0.0004	0.5530	0.0143	0.0560	0.0014	446	3	447	12	451	56	100
PM19-26-14	0.399	7	39	97	0.0730	0.0004	0.5519	0.0125	0.0548	0.0012	454	3	446	10	406	50	98
PM19-26-15	0.426	11	62	146	0.0722	0.0004	0.5554	0.0086	0.0558	0.0008	449	3	449	7	444	32	100
PM19-26-16	0.372	8	39	105	0.0723	0.0005	0.5533	0.0134	0.0555	0.0013	450	3	447	11	434	52	99
PM19-26-17	0.355	7	33	93	0.0724	0.0004	0.5544	0.0107	0.0556	0.0011	450	3	448	9	435	42	100
PM19-26-18	0.445	13	78	175	0.0724	0.0004	0.5594	0.0085	0.0560	0.0008	451	3	451	7	453	32	100
PM19-26-19	0.451	11	65	144	0.0728	0.0004	0.5561	0.0130	0.0554	0.0013	453	3	449	11	429	50	99
PM19-26-20	0.530	18	104	196	0.0793	0.0005	1.1643	0.0253	0.1064	0.0020	492	3	784	17	1739	34	41
PM19-26-21	0.501	15	79	157	0.0809	0.0005	1.1962	0.0262	0.1072	0.0022	502	3	799	17	1752	37	41
PM19-26-22	0.440	10	62	140	0.0723	0.0004	0.5589	0.0092	0.0561	0.0009	450	3	451	7	454	35	100
PM19-26-23	0.473	11	53	113	0.0793	0.0005	1.3038	0.0207	0.1193	0.0018	492	3	847	13	1946	27	28
PM19-26-24	0.411	12	49	119	0.0791	0.0006	1.5809	0.0600	0.1449	0.0047	491	4	963	37	2287	56	4
Sample PM19-CN2, granite porphyry, 45° 58' 57" N, 118° 17' 37" E																	
PM19-CN2-1	0.665	28	247	371	0.0711	0.0007	0.5480	0.0115	0.0559	0.0011	443	5	444	9	449	43	100
PM19-CN2-2	0.678	25	223	329	0.0711	0.0008	0.5506	0.0135	0.0562	0.0013	443	5	445	11	460	50	100
PM19-CN2-3	0.624	16	143	229	0.0658	0.0007	0.5947	0.0153	0.0656	0.0016	411	4	474	12	792	52	85
PM19-CN2-4	0.600	17	139	232	0.0711	0.0007	0.5564	0.0154	0.0568	0.0015	443	5	449	12	483	59	99
PM19-CN2-5	0.680	22	198	291	0.0714	0.0008	0.5551	0.0135	0.0564	0.0013	445	5	448	11	468	51	99
PM19-CN2-6	0.899	26	282	314	0.0738	0.0009	0.5827	0.0130	0.0572	0.0012	459	5	466	10	501	45	98
PM19-CN2-7	0.583	14	107	183	0.0734	0.0008	0.6129	0.0200	0.0605	0.0019	457	5	485	16	623	68	94
PM19-CN2-8	0.910	43	476	523	0.0721	0.0007	0.7835	0.0130	0.0788	0.0012	449	5	587	10	1167	31	69
PM19-CN2-9	0.846	30	345	408	0.0662	0.0008	0.6099	0.0128	0.0668	0.0012	413	5	483	10	832	38	83
PM19-CN2-10	0.862	39	427	495	0.0711	0.0007	0.5472	0.0115	0.0558	0.0011	443	4	443	9	446	45	100
PM19-CN2-11	0.888	33	377	424	0.0709	0.0007	0.5481	0.0114	0.0561	0.0011	441	5	444	9	456	42	99
PM19-CN2-12	0.836	30	326	390	0.0710	0.0007	0.5542	0.0121	0.0566	0.0012	442	4	448	10	477	46	99
PM19-CN2-13	0.853	34	383	449	0.0677	0.0007	0.5936	0.0101	0.0636	0.0010	422	4	473	8	728	33	88
PM19-CN2-14	0.653	25	204	313	0.0716	0.0009	0.5520	0.0176	0.0559	0.0017	446	5	446	14	450	66	100
PM19-CN2-15	0.711	40	419	589	0.0621	0.0006	0.5034	0.0086	0.0588	0.0009	388	4	414	7	561	34	93

(Continued)

Table 1. (Continued)

Sample no.	Content (ppm)				Ratio						Age (Ma)				Concordance (%)		
	$^{232}\text{Th}/^{238}\text{U}$	Pb	Th	U	$^{206}\text{Pb}/^{238}\text{U}$	1σ	$^{207}\text{Pb}/^{235}\text{U}$	1σ	$^{207}\text{Pb}/^{206}\text{Pb}$	1σ	$^{206}\text{Pb}/^{238}\text{U}$	1σ	$^{207}\text{Pb}/^{235}\text{U}$	1σ		$^{207}\text{Pb}/^{206}\text{Pb}$	1σ
PM19-CN2-16	0.795	27	290	365	0.0640	0.0007	0.7008	0.0132	0.0794	0.0014	400	4	539	10	1183	34	65
PM19-CN2-17	0.721	28	257	357	0.0717	0.0008	0.5559	0.0114	0.0562	0.0011	447	5	449	9	460	43	100
PM19-CN2-18	0.726	20	192	264	0.0713	0.0008	0.5559	0.0149	0.0566	0.0014	444	5	449	12	475	55	99
PM19-CN2-19	0.647	19	161	249	0.0714	0.0007	0.5522	0.0146	0.0561	0.0014	445	5	446	12	455	56	100
PM19-CN2-20	0.960	35	418	435	0.0711	0.0007	0.5521	0.0119	0.0563	0.0011	443	5	446	10	464	44	99
PM19-CN2-21	0.786	19	193	245	0.0711	0.0008	0.5561	0.0160	0.0567	0.0015	443	5	449	13	480	59	99
PM19-CN2-22	0.885	35	394	445	0.0711	0.0007	0.5545	0.0103	0.0565	0.0010	443	5	448	8	473	38	99
PM19-CN2-23	0.792	18	177	224	0.0710	0.0008	0.5495	0.0192	0.0562	0.0018	442	5	445	15	459	73	99
PM19-CN2-24	0.779	35	345	443	0.0679	0.0007	0.8334	0.0237	0.0890	0.0024	423	4	615	17	1405	52	55
PM19-CN2-25	0.654	24	226	345	0.0637	0.0007	0.6709	0.0166	0.0764	0.0016	398	4	521	13	1105	43	69
PM19-CN2-26	0.807	19	199	246	0.0713	0.0007	0.5595	0.0165	0.0569	0.0016	444	5	451	13	488	63	98
PM19-CN2-27	0.620	12	103	166	0.0713	0.0008	0.5483	0.0232	0.0558	0.0023	444	5	444	19	445	94	100
PM19-CN2-28	1.076	39	514	478	0.0712	0.0007	0.5541	0.0100	0.0565	0.0010	443	5	448	8	470	37	99
PM19-CN2-29	0.722	20	219	303	0.0606	0.0008	0.5161	0.0127	0.0618	0.0014	379	5	423	10	667	47	88
PM19-CN2-30	0.757	24	229	303	0.0707	0.0007	0.5459	0.0165	0.0560	0.0016	440	5	442	13	452	64	100
PM19-CN2-31	0.632	22	207	327	0.0622	0.0007	0.5415	0.0130	0.0632	0.0014	389	4	439	11	714	48	87
PM19-CN2-32	0.464	21	174	374	0.0536	0.0008	0.4728	0.0126	0.0640	0.0016	337	5	393	10	740	52	83

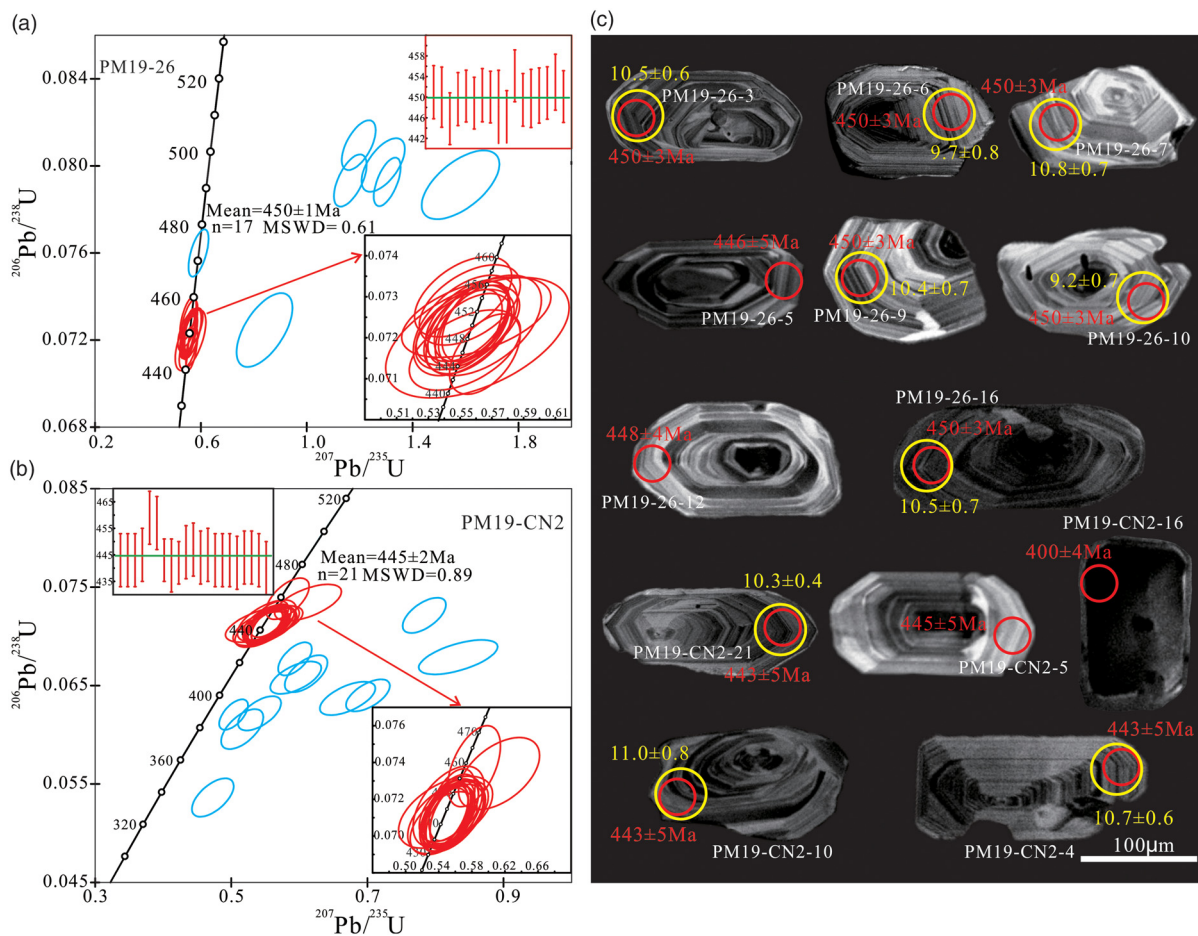


Fig. 3. (Colour online) LA-ICP-MS zircon U-Pb concordia diagrams for samples (a) PM19-26 and (b) PM19-CN2 from the Mante Aobao granite porphyry in the East Ujimqin Banner area. (c) Representative cathodoluminescence (CL) images, U-Pb ages and Hf isotopic compositions of zircons from samples PM19-26 and PM19-CN2. The red circles are 32 μm in diameter and show the location of the U-Pb analytical sites; the yellow circles are 44 μm in diameter and show the location of the Lu-Hf isotopes analytical sites.

Table 2. Zircon Hf isotope compositions of the Mante Aobao granite porphyry in East Ujimqin Banner, Inner Mongolia

Sample no.	Age (Ma)	¹⁷⁶ Yb/ ¹⁷⁷ Hf	¹⁷⁶ Lu/ ¹⁷⁷ Hf	¹⁷⁶ Hf/ ¹⁷⁷ Hf	±2σ	(¹⁷⁶ Hf/ ¹⁷⁷ Hf) _i	ε _{Hf} (t)	T _{DM1} (Ma)	T _{DM2} (Ma)	f _{Lu/Hf}
PM19-26-3	450	0.025812	0.001133	0.282808	0.000018	0.282798	10.5	632	739	-0.97
PM19-26-6	450	0.011125	0.001039	0.282783	0.000022	0.282774	9.7	665	794	-0.97
PM19-26-7	450	0.020873	0.001267	0.282818	0.00002	0.282807	10.8	620	719	-0.96
PM19-26-9	450	0.013647	0.000601	0.282800	0.00002	0.282795	10.4	634	747	-0.98
PM19-26-10	450	0.024069	0.000563	0.282767	0.00002	0.282762	9.2	679	821	-0.98
PM19-26-16	450	0.022945	0.000671	0.282805	0.00002	0.282799	10.5	628	737	-0.98
PM19-26-17	450	0.016751	0.001801	0.282792	0.00002	0.282777	9.7	666	788	-0.95
PM19-26-22	450	0.026654	0.000916	0.282809	0.00002	0.282801	10.6	626	733	-0.97
PM19-CN2-1	445	0.028112	0.000713	0.282799	0.00002	0.282793	10.2	637	755	-0.98
PM19-CN2-2	445	0.021054	0.000846	0.282828	0.00002	0.282821	11.2	599	691	-0.97
PM19-CN2-4	445	0.022672	0.001413	0.282819	0.000017	0.282807	10.7	621	723	-0.96
PM19-CN2-10	445	0.018745	0.001257	0.282827	0.000023	0.282817	11.0	607	702	-0.96
PM19-CN2-20	445	0.014277	0.000964	0.282816	0.00002	0.282808	10.7	617	721	-0.97
PM19-CN2-21	445	0.033711	0.001648	0.282811	0.000012	0.282797	10.4	636	745	-0.95
PM19-CN2-22	445	0.027683	0.000873	0.282776	0.00002	0.282769	9.3	672	810	-0.97
PM19-CN2-28	445	0.030549	0.001311	0.282823	0.000025	0.282812	10.9	613	712	-0.96

(¹⁷⁶Hf/¹⁷⁷Hf)_i = (¹⁷⁶Hf/¹⁷⁷Hf)_{initial} = (¹⁷⁶Hf/¹⁷⁷Hf)_s - (¹⁷⁶Lu/¹⁷⁷Hf)_s × (e^{λt} - 1); ε_{Hf}(t) = [(¹⁷⁶Hf/¹⁷⁷Hf)_s - (¹⁷⁶Lu/¹⁷⁷Hf)_s × (e^{λt} - 1)] / [(¹⁷⁶Hf/¹⁷⁷Hf)_{CHUR,0} - (¹⁷⁶Lu/¹⁷⁷Hf)_{CHUR} × (e^{λt} - 1)] × 10 000; f_{Lu/Hf} = [(¹⁷⁶Lu/¹⁷⁷Hf)_s / (¹⁷⁶Lu/¹⁷⁷Hf)_{Chondrite} - 1] × 100%; T_{DM1} = 1/λ × ln[1 + ((¹⁷⁶Hf/¹⁷⁷Hf)_s - (¹⁷⁶Hf/¹⁷⁷Hf)_{DM}) / ((¹⁷⁶Lu/¹⁷⁷Hf)_s - (¹⁷⁶Lu/¹⁷⁷Hf)_{DM})]; T_{DM2} = T_{DM1} - (T_{DM1} - t) × [(f_{CC} - f_S) / (f_{CC} - f_{DM})], where t is weighted age of zircon in the sample; λ is ¹⁷⁶Lu β-decay constant; (¹⁷⁶Hf/¹⁷⁷Hf)_i is initial ¹⁷⁶Hf/¹⁷⁷Hf ratio in samples; (¹⁷⁶Hf/¹⁷⁷Hf)_s and (¹⁷⁶Lu/¹⁷⁷Hf)_s are values measured in samples; ε_{Hf}(t) and f_{Lu/Hf} are deviation of Hf isotopic composition from chondrites; (¹⁷⁶Hf/¹⁷⁷Hf)_{CHUR,0} and (¹⁷⁶Lu/¹⁷⁷Hf)_{CHUR} are evolution of the (¹⁷⁶Hf/¹⁷⁷Hf) and (¹⁷⁶Lu/¹⁷⁷Hf) ratios in chondritic uniform reservoir, respectively; (¹⁷⁶Hf/¹⁷⁷Hf)_{DM} and (¹⁷⁶Lu/¹⁷⁷Hf)_{DM} are (¹⁷⁶Hf/¹⁷⁷Hf) and (¹⁷⁶Lu/¹⁷⁷Hf) ratios in depleted mantle (DM), respectively; T_{DM1} is single-stage evolutionary depleted mantle Hf model age of source rock; T_{DM2} is crust model age; f_{CC}, f_S and f_{DM} are present f_{Lu/Hf} values of continental crust, samples and depleted mantle, respectively. λ = 1.867 × 10⁻¹¹ a⁻¹; (¹⁷⁶Hf/¹⁷⁷Hf)_{CHUR,0} = 0.282772; (¹⁷⁶Lu/¹⁷⁷Hf)_{CHUR} = 0.03321 (Blichert-Toft & Albarede, 1997); (¹⁷⁶Hf/¹⁷⁷Hf)_{DM} = 0.28325, (¹⁷⁶Lu/¹⁷⁷Hf)_{DM} = 0.03824 (Griffin et al. 2000); f_{CC} = -0.55 (average crust, Griffin et al. 2000); f_{DM} = 0.1566 (Griffin et al. 2000).

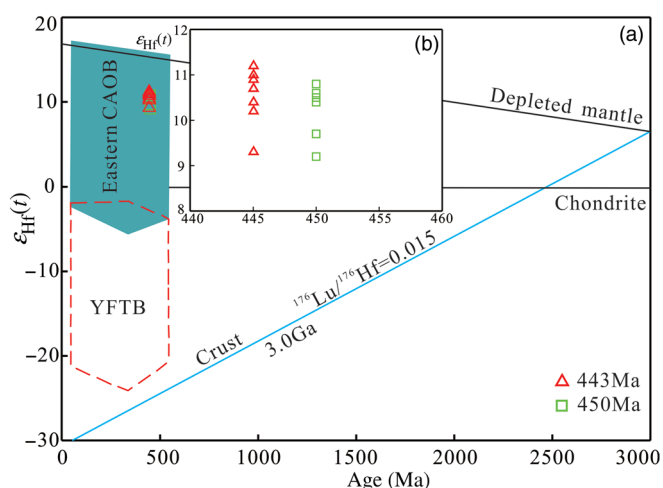


Fig. 4. (Colour online) Diagrams of zircon ε_{Hf}(t) versus crystallization age for the Mante Aobao granite porphyry: (a) 0–3000 Ma, with fields for the Eastern Central Asian Orogenic Belt (CAOB) (Xiao et al. 2004; Chen et al. 2009) and the Yanshan Fold and Thrust Belt (YFTB) (Yang et al. 2006); and (b) close-up of the Mante Aobao granite porphyry data for age 440–460 Ma.

(3.06–3.92 wt%). Total alkalis (K₂O+Na₂O) range from 7.26 to 8.23 wt%, plotting in the granite field on the total alkali-silica (TAS) diagram (Middlemost, 1994; Fig. 5a). Using the K₂O versus SiO₂ classification diagram, the samples belong to the medium- to high-K calc-alkaline series (Rickwood, 1989; Fig. 5b). They have relatively high Al₂O₃ contents (13.48–14.59 wt%), and vary from metaluminous to weakly peraluminous (aluminous saturation

index A/CNK, molar Al₂O₃/(CaO+K₂O+Na₂O), of 0.98–1.11) (Peccerillo & Taylor, 1976; Fig. 5c), with uniform alumina saturation indices (ASI) of 0.73–0.84 (Table 3). The samples also exhibit low FeO^T (2.13–2.58 wt%) and MgO (0.57–0.81 wt%) contents, which means they have magnesian granitic affinities according to the classification scheme of Frost et al. (2001) (Fig. 5d).

Total rare earth element (REE) concentrations for the Mante Aobao granite porphyry range over 132–149 ppm (mean, 141 ppm). Chondrite-normalized REE patterns (Sun & McDonough, 1989; Fig. 6a) exhibit enrichment of light REEs (LREEs) with (La/Yb)_N ratios of 4.68–5.77, and have moderate negative Eu anomalies with Eu/Eu* ratios of 0.52–0.63, as well as a greater differentiation of LREEs ((La/Sm)_N = 3.1–3.6) compared with heavy REEs (HREEs) ((Gd/Yb)_N = 1.0–1.1; Fig. 6a). On a primitive mantle-normalized spidergram (Sun & McDonough, 1989; Fig. 6b), the Mante Aobao granite porphyry samples are enriched with large-ion lithophile elements (LILEs, e.g. U, Th, Rb and K), light REEs and Pb, and are depleted in high-field-strength elements (HFSEs, e.g. Nb, Ta, P and Ti); troughs for Sr and Ti may be related to plagioclase and Fe–Ti oxide remaining in the source or, for the latter, to the early extraction of Fe–Ti phases. The zircon saturation temperatures (T_{Zr}) for the Mante Aobao granite porphyry, calculated using the method proposed by Watson & Harrison (1983), are 802–823°C (Table 3).

5. Discussion

5.a. Age of the Mante Aobao granite porphyry

These are the first isotopic crystallization ages obtained for the Mante Aobao granite porphyry. Relying only on geological features

Table 3. Chemical compositions and main geochemical parameters of the Mante Aobao granite porphyry in East Ujimqin Banner, Inner Mongolia

Sample No.	PM19-9	PM19-10	PM19-14	PM19-15	PM19-16	PM19-18	PM19-20	PM19-21	PM19-22	PM19-25	PM19-27
Major elements											
SiO ₂ (wt%)	72.01	71.76	72.09	71.69	71.9	71.99	71.9	71.79	72.16	72.33	72.13
TiO ₂ (wt%)	0.35	0.33	0.36	0.35	0.35	0.34	0.36	0.35	0.37	0.33	0.37
Al ₂ O ₃ (wt%)	14.14	13.76	13.78	13.77	13.71	13.93	13.89	14.59	13.6	13.48	13.86
FeO (wt%)	0.85	0.80	0.42	0.90	0.83	0.93	0.78	0.65	0.78	0.93	0.87
Fe ₂ O ₃ (wt%)	1.70	1.98	2.12	1.82	1.82	1.40	1.90	1.78	1.97	1.33	1.49
FeO ^T (wt%)	2.38	2.58	2.33	2.54	2.47	2.19	2.49	2.25	2.55	2.13	2.21
MnO (wt%)	0.05	0.06	0.08	0.07	0.08	0.07	0.08	0.05	0.09	0.07	0.09
MgO (wt%)	0.57	0.59	0.66	0.69	0.65	0.75	0.63	0.62	0.78	0.81	0.62
CaO (wt%)	1	1.6	1.21	1.1	1.07	0.96	0.99	1.04	1.37	1.95	1.14
Na ₂ O (wt%)	4.52	4.62	4.81	4.23	4.72	4.64	4.57	4.73	4.94	3.61	5.01
K ₂ O (wt%)	3.51	3.25	3.08	3.92	3.45	3.59	3.64	3.21	2.65	3.65	3.06
P ₂ O ₅ (wt%)	0.08	0.08	0.08	0.09	0.09	0.09	0.09	0.08	0.08	0.07	0.08
LOI (wt%)	1	0.99	1.13	1.27	1.15	1.15	1.07	0.99	0.98	1.31	1.06
Total (wt%)	99.91	99.94	99.9	100.04	99.95	99.98	100.02	99.98	99.89	100.01	99.91
K ₂ O+Na ₂ O (wt%)	8.03	7.87	7.89	8.15	8.17	8.23	8.21	7.94	7.59	7.26	8.07
K ₂ O/Na ₂ O	0.78	0.70	0.64	0.93	0.73	0.77	0.80	0.68	0.54	1.01	0.61
Mg no.	30	29	34	33	32	38	31	33	35	40	33
A/NK ^a	1.26	1.24	1.23	1.23	1.19	1.21	1.21	1.30	1.24	1.36	1.20
A/CNK ^b	1.08	0.98	1.02	1.04	1.02	1.05	1.05	1.11	1.01	1.00	1.02
ASI ^c	0.79	0.81	0.82	0.81	0.84	0.83	0.82	0.77	0.81	0.73	0.83
FeO ^T /MgO ^d	4.17	4.38	3.53	3.68	3.80	2.92	3.95	3.63	3.27	2.63	3.56
T _{Zr} (°C) ^e	819	808	822	819	818	821	821	823	818	812	819
Trace elements (ppm)											
Cr	4.29	5.70	4.09	7.05	5.30	5.39	17.06	8.81	7.07	8.55	4.94
Ni	3.70	5.08	3.18	4.95	4.06	3.60	15.36	6.65	5.60	6.62	5.58
Rb	108.87	91.39	118.24	129.16	117.21	107.43	113.30	98.30	72.50	150.28	99.58
Ba	592.28	503.30	512.66	708.50	632.78	606.18	615.00	552.00	474.79	663.49	525.28
Th	10.25	9.41	10.24	10.32	10.81	8.56	9.89	10.47	7.79	10.78	10.63
U	2.88	2.66	2.87	2.77	2.79	2.40	2.57	2.70	1.76	2.98	2.57
Nb	7.03	6.60	7.29	7.27	7.62	7.07	7.00	6.99	7.19	7.00	7.52
Sr	88.70	103.83	128.06	112.87	113.01	100.61	189.65	117.65	96.97	243.80	128.49
Zr	223.00	222.90	245.10	232.60	235.90	236.20	236.80	227.20	239.00	222.70	241.20
Hf	7.37	7.50	9.33	8.24	8.13	8.17	8.17	7.79	8.12	7.83	8.42
Co	2.49	2.84	2.51	1.80	1.44	2.99	2.58	2.58	2.06	3.87	2.69
Pb	17.26	13.79	8.62	16.77	16.94	17.44	24.41	21.49	16.94	60.22	55.60
10 000×Ga/Al	2.07	2.11	2.17	2.16	2.26	2.04	2.24	2.15	2.16	2.38	2.27
Zr+Nb+Ce+Y	301	298	322	310	319	312	3181	308	321	297	320
Nb/Ta	8.51	9.78	9.66	9.77	8.30	9.13	9.54	9.90	9.07	8.27	9.75
Zr/Hf	30.26	29.74	26.26	28.24	29.01	28.92	29.00	29.18	29.45	28.45	28.66
Th/U	3.55	3.54	3.56	3.72	3.87	3.57	3.85	3.87	4.41	3.62	4.14
Rare earth elements (ppm)											
La	21.61	21.06	21.59	21.00	22.13	20.50	24.21	24.12	23.13	19.60	21.39
Ce	42.62	41.71	42.60	44.08	45.97	42.63	47.36	47.56	46.50	40.23	44.90

(Continued)

Table 3. (Continued)

Sample No.	PM19-9	PM19-10	PM19-14	PM19-15	PM19-16	PM19-18	PM19-20	PM19-21	PM19-22	PM19-25	PM19-27
Pr	5.16	4.99	5.38	5.13	5.45	5.16	5.66	5.51	5.52	4.79	5.08
Nd	19.82	19.37	21.36	19.58	21.28	19.69	21.93	21.24	21.60	18.67	19.74
Sm	4.20	4.04	4.47	4.12	4.45	4.09	4.39	4.34	4.59	4.00	4.18
Eu	0.83	0.81	0.86	0.80	0.88	0.77	0.85	0.86	0.90	0.69	0.87
Gd	4.22	4.11	4.35	3.89	4.26	3.80	4.13	3.92	4.27	3.94	4.07
Tb	0.76	0.75	0.79	0.74	0.78	0.69	0.75	0.73	0.78	0.74	0.72
Dy	4.75	4.64	4.81	4.39	4.63	4.35	4.55	4.37	4.69	4.61	4.48
Y	28.23	27.14	27.23	25.88	29.22	25.74	26.85	26.00	28.12	26.99	26.62
Ho	1.00	1.00	1.00	0.95	1.02	0.92	0.95	0.92	1.03	0.97	0.95
Er	3.01	2.93	3.01	2.77	3.08	2.83	2.90	2.79	3.13	2.93	2.85
Tm	0.49	0.49	0.49	0.46	0.51	0.49	0.48	0.47	0.51	0.48	0.47
Yb	3.18	3.08	3.18	2.96	3.30	3.14	3.18	3.00	3.33	3.14	3.04
Lu	0.52	0.52	0.52	0.48	0.54	0.53	0.51	0.51	0.53	0.51	0.50
ΣREE	140.38	136.64	141.63	137.23	147.48	135.34	148.69	146.33	148.62	132.26	139.86
(La/Yb) _N ^f	4.87	4.90	4.86	5.08	4.81	4.68	5.47	5.77	4.99	4.48	5.05
(La/Sm) _N	3.32	3.36	3.12	3.29	3.21	3.23	3.56	3.58	3.26	3.17	3.30
(Gd/Lu) _N	1.00	0.98	1.03	0.99	0.98	0.89	1.00	0.96	1.00	0.96	1.00
Eu/Eu* ^g	0.60	0.60	0.59	0.60	0.61	0.59	0.60	0.63	0.61	0.52	0.63
DI	89	87	89	89	89	90	89	89	87	85	89
Corundum	0.0	0.17	0.53	0.79	0.49	0.89	0.86	1.65	0.31	0.29	0.43

^a A/NK = molar Al₂O₃/(Na₂O+K₂O); ^b A/CNK = molar Al₂O₃/(CaO+Na₂O+K₂O); ^c Aluminium saturation index ASI = Al/(Ca - 1.67P + Na + K); ^d FeO^T = FeO + 0.8998 × Fe₂O₃; ^e T_{Zr} (°C) = 12 900/[2.95+0.85M+ln(496 000/Zr_{melt})] - 273.15, where M = (Na+K+2Ca)/(Al×Si), mole ratio and Zr_{melt} is the Zr content in the magma (Watson & Harrison, 1983); ^f (La/Yb)_N is chondrite-normalized ratio; ^g Eu/Eu* = EuN/(SmN × GdN)/2, where N denotes chondrite normalization. The chondrite values are from Sun & McDonough (1989).

(Fig. 2a, b), previous researchers suggested that its formation age should be older than that of the volcanic rocks associated with the upper Carboniferous – lower Permian Baoligaomiao Formation. The zircon U–Pb ages indicate that the emplacement of the granite porphyry occurred at 445–450 Ma, which means it formed in the Late Ordovician Period, contemporaneous with other plutonic rocks in the Uliastai continental margin of the north-central Xing’an–Mongolian Orogenic Belt (Fig. 1b) including the granodiorite at Gilgalantu (433–497 Ma) (Yang *et al.* 2017), the complex massif at Geriaobao (449 Ma) (Zhao *et al.* 2012), the gabbro in the western sector of the Shamai area (449 Ma) (Yang, 2016), the granodiorite in the western Mandubaolige area (446–461 Ma) (Yang, 2016), and the gabbro in the East Ujimiqin Banner area at Chaobuleng (450–461 Ma) (Li *et al.* 2016).

5.b. Classification of the Mante Aobao granite porphyry

Chappell & White (1974, 1992) first proposed the S-I classification for granites and, subsequently, the ‘alphabet classification’ of S-, I-, M- and A-type granites evolved (Bonin, 2007). The Mante Aobao granite porphyry is geochemically distinct from M-type granites, which are characterized by low K₂O values (typically <1 wt%) (Bonin, 2007), relatively low alumina saturation indices (0.73–0.84), low 10 000 × Ga/Al values (2.04–2.38), low HFSE contents (Zr+Nb+Ce+Y = 297–322 ppm), low (Na₂O+K₂O)/CaO ratios (3.72–8.57) and low FeO^T/MgO ratios (2.34–4.38), distinguishing

them from A-type granites (Fig. 7a, b) (Whalen *et al.* 1987). Moreover, most samples plot in the field of fractionated granites (FG) (Fig. 7a, b).

The samples of granite porphyry in this study are calc-alkaline to high-K calc-alkaline, and metaluminous to weakly peraluminous (A/CNK = 0.98–1.11), which are characteristics of I-type granites (Chappell & White, 1974). Generally, trace elements such as Rb, Y and Th are commonly used for distinguishing I- and S-type granites (Li *et al.* 2007). In Th and Y versus Rb diagrams (Chappell & White, 1992; Li *et al.* 2007; Zhu *et al.* 2009; Fig. 7c, d), our samples exhibit a distinct I-type trend. The amounts of differentiation index (DI) and corundum in the CIPW norm calculations are almost entirely within the range of 85–90% and 0.17–1.65%, respectively (with only one sample having >1% corundum), consistent with highly fractionated I-type granites (Chappell & White, 2001). In addition, the bulk zirconium saturation temperatures calculated for the Mante Aobao granite porphyry (Table 3, 802–823°C) are higher than those indicative of mean S-type granite temperatures (i.e. 764°C) (Pearce *et al.* 1984). Accordingly, the Mante Aobao granite porphyry can be classified as a highly fractionated I-type granite.

5.c. Petrogenesis of the Mante Aobao granite porphyry

Parental magmas of highly fractionated I-type granites may be produced by: (1) fractional crystallization from mantle-derived mafic

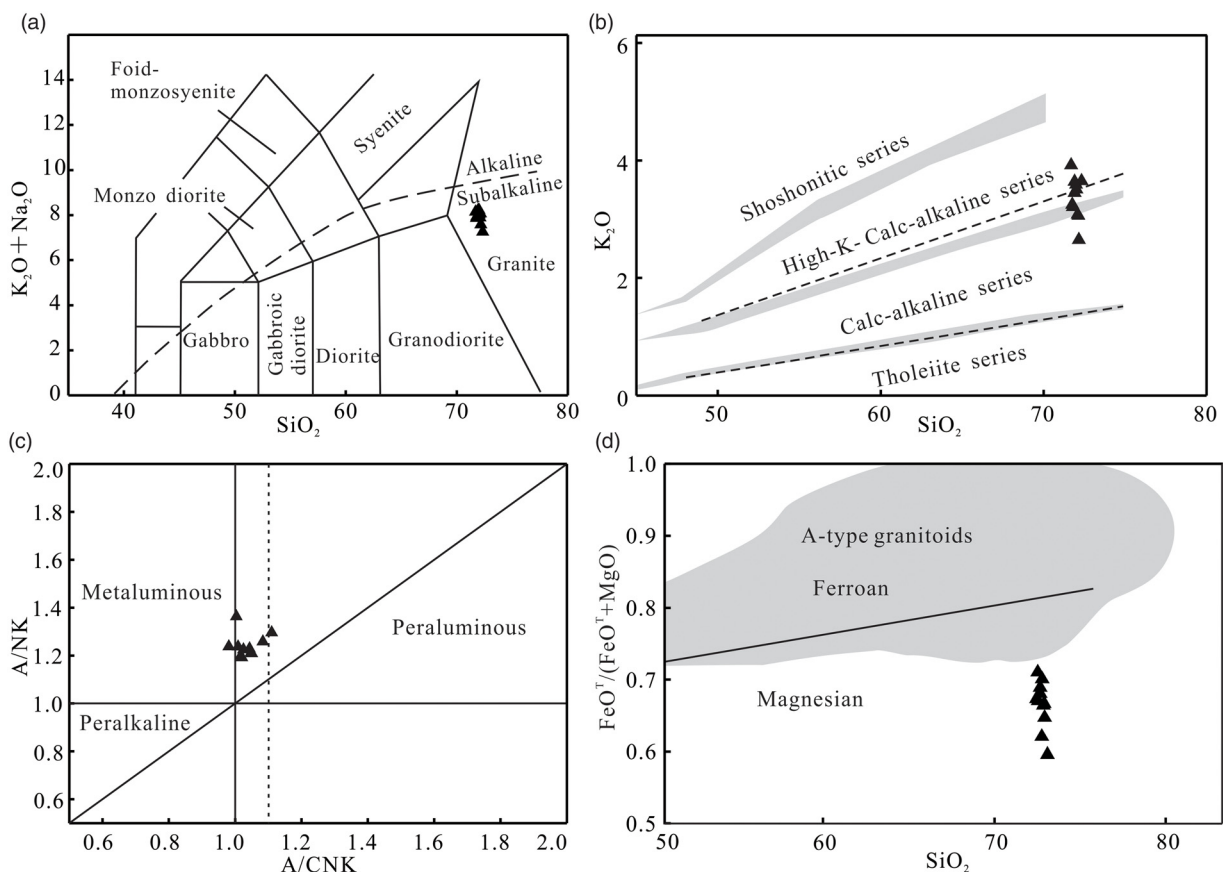


Fig. 5. Geochemical diagrams for the Mante Aobao granite porphyry in East Ujimqin Banner. (a) TAS diagram for chemical classification (Middlemost, 1994) and alkalinity index (after Irvine & Baragar, 1971); (b) K_2O versus SiO_2 diagram (Rickwood, 1989); (c) A/NK versus A/CNK diagram (Peccerillo & Taylor, 1976); and (d) $FeO^7/(FeO^7+MgO)$ versus SiO_2 (Frost *et al.* 2001). A-type granite field after Frost *et al.* (2001).

magma (Chappell, 1999; Wyborn *et al.* 2001); (2) mixing between crust-derived felsic and mantle-derived mafic magmas (Wu *et al.* 2005a; Li *et al.* 2007; Zhu *et al.* 2009); and (3) partial melting of crustal material, followed by fractional crystallization (Chappell & White, 2001; Wu *et al.* 2005a). The Mante Aobao I-type granite porphyry samples have relatively low MgO (0.57–0.81 wt%), Mg no. (29–40), Cr (4.09–17.06 ppm) and Ni (3.18–15.36 ppm) contents, inconsistent with the compositional characteristics of a mafic melt (Baker *et al.* 1995; Valley *et al.* 2005). On the basis of experimental petrology, hydrous, medium- to high-K mafic magmas can only fractionate to produce 12–25 wt% of a granitic differentiation product (Sisson *et al.* 2005), meaning that large volumes of mafic rocks would be required to be coeval and cogenetic with the granites. We consider it unlikely that the primary magma of the Mante Aobao granite porphyry was generated directly from fractional crystallization of mafic magma because the SiO_2 contents are extremely high (>71%); furthermore, there is a lack of contemporaneous large-scale mafic igneous rocks in the area. The magmatic mixing of mantle- and crust-derived melts would produce a wide range of isotopic and geochemical signatures. This is inconsistent with the narrow range of zircon $\epsilon_{Hf}(t)$ values (+9.2 to +11.2) and the chemical composition (Table 3) of the Mante Aobao granite porphyry. Moreover, flow structures or mafic enclaves, which are two significant indicators of magma mixing (Perugini & Poli, 2012), have not been found in the Mante Aobao granite porphyry. Petrographic textures, such as quartz ocelli rimmed by hornblende and/or biotite and acicular apatite, which are typical

of magma mixing (Hibbard, 1991; Baxter & Feely, 2002), are also absent (Fig. 2b–d). Hence, the magma mixing model is inapplicable to the Mante Aobao granite porphyry. In general, the partial melting of mafic crustal materials accounts for the origin of I-type granites, as commonly documented by field observations, geochemical and experimental data (Chappell, 1999). The Mante Aobao granite porphyry samples display enrichment in LREEs relative to HREEs, with negative Eu anomalies and relatively flat HREE patterns. All these features, combined with the relatively high SiO_2 contents, suggests that it is a crust-derived granite. Some trace element ratios (e.g. Nb/Ta, Zr/Hf and Th/U) are also useful to reveal the source rocks of granitic magmas. The similarity of the Nb/Ta (8.27–9.9; mean, 9.24), Zr/Hf (26.26–30.26; mean, 28.83) and Th/U (3.54–4.41; mean, 3.79) values between the Mante Aobao I-type granites and the bulk continental crust (Nb/Ta = 11, Zr/Hf = 33 and Th/U = 4) (Taylor & McLennan, 1985, p.312) is also consistent with a crustal origin. Furthermore, the zircons exhibit positive $\epsilon_{Hf}(t)$ values ranging from +9.2 to +11.2, and yield two-stage Hf model ages (T_{DM2}) of 691–821 Ma, implying that the primitive magma was derived from juvenile crust, similar to the magma sources of the Palaeozoic – lower Mesozoic magmatic rocks in the south accretionary margin of the Siberian Craton which derived from depleted mantle or juvenile crust materials (Wu *et al.* 1999, 2000, 2003, 2007; Chen *et al.* 2000; Jahn *et al.* 2000, 2004; Sui *et al.* 2007; Miao *et al.* 2008; Liu *et al.* 2012). Moreover, in the La/Sm versus La diagram (Fig. 8a) and in the Zr/Nb versus Zr diagram (Fig. 8b) the samples from the Mante Aobao granite

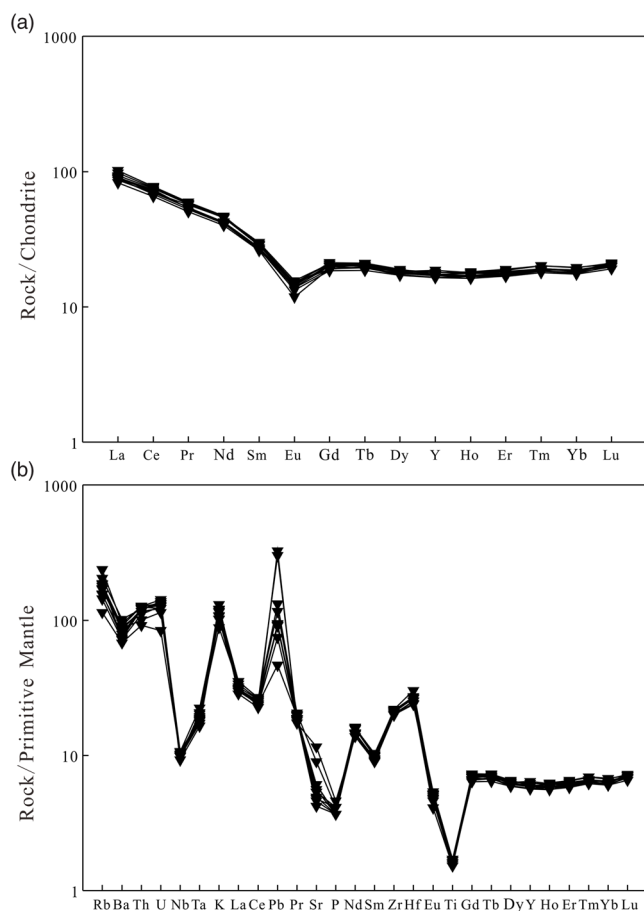


Fig. 6. (a) Chondrite-normalized REE diagram and (b) primitive mantle-normalized trace-element spider diagram for the Mante Aobao granite porphyry in East Ujimqin Banner. Primitive mantle and chondrite values from Sun & McDonough (1989).

porphyry define nearly horizontal trends, suggesting that fractional crystallization played a more important role during the magmatic evolution of the granites. The samples show significant depletion in Nb, Ta, Ti, Ba, Sr, P and Eu, which suggests that rutile, Fe–Ti oxides and apatite were rare in or absent from the magma sources. The pronounced depletion in these elements also implies fractional crystallization of plagioclase, K-feldspar and apatite during magmatic evolution. In summary, the granite porphyry was generated by partial melting of Neoproterozoic juvenile crust and subsequently underwent fractional crystallization during evolution and ascent of the magma. Combined with the relatively high zircon saturation temperatures (mostly 802–823°C; Table 3), it is suggested that the heat source for partial melting may have been provided by the underplating of mantle-derived magmas during the Late Ordovician Period.

5.d. Tectonic setting

Although small, the Mante Aobao granite porphyry offers important insights into the tectonic evolution of the Xing’an–Mongolian Orogenic Belt. The U–Pb ages of 445–450 Ma demonstrate that a Late Ordovician magmatic event occurred in the East Ujimqin Banner area. To identify the tectonic setting of the Mante Aobao granite porphyry, we use plots of (La/Yb)_N versus Yb_N, Sr/Y versus Y, the (Ta×3)–(Rb/30)–Hf triangular diagram, and Rb versus (Y+Nb) (Harris *et al.* 1986; Defant & Drummond,

1990; Fig. 9a–d). Most samples plot in the arc and volcanic-arc fields on these tectonic discrimination diagrams. Furthermore, in the Th/Yb versus Ta/Yb and La/Yb versus Th/Yb diagrams (Pearce *et al.* 1984; Condie, 1989; Gorton & Schandl, 2000; Fig. 9e, f), all samples plot within the active continental margin field. In Figure 1b, we have synthesized data from numerous lower Palaeozoic magmatic rocks with zircon U–Pb ages of 433–496 Ma, which extend in a NE direction along the East Ujimqin Banner, Geri Obao and Erenhot axis towards Mongolia (Cui *et al.* 2008; Wilhem *et al.* 2012; Zhao *et al.* 2012; Yang *et al.* 2014; Zhu *et al.* 2014; Li *et al.* 2016). All these rocks have typical arc signatures, and the geochemical data for the Mante Aobao granite porphyry presented in this study share these same characteristics (Fig. 9a, b). Accordingly, the Mante Aobao granite porphyry, as well as the other almost coeval plutons, formed in an extensive subduction-related continental margin-arc setting that is consistent with generation during subduction of the Paleo-Asian Ocean.

Previous studies have shown that the Xing’an–Mongolian Orogenic Belt underwent a series of tectonic events, including oceanic plate subduction, crustal accretion, multi-block collision and post-orogenic extension during the early Palaeozoic Era, resulting in several accreted tectono-magmatic belts (Xiao *et al.* 2003; Xu *et al.* 2015). In southern Mongolia, north of the study area, a series of large-scale subduction–accretion episodes took place between the Neoproterozoic and the early Palaeozoic eras. The Mongolian arc, now located in the border region between China and Mongolia, potentially extends from western Mongolia and connects with the Toudaoqiao–Gaxian–Xinlin ophiolite belt in the east. In terms of its tectonic position, the Mante Aobao granite porphyry may therefore occupy the extension of the southern margin of the Mongolian arc into China (Badarch *et al.* 2002; Eizenhöfer *et al.* 2014, 2015; Xu *et al.* 2015, 2017). However, according to existing data, ophiolites related to the Mongolian arc formed principally during Neoproterozoic–Cambrian time. For example, the formation age of the ophiolites in the western sector of the arc at Bayankhongor in central Mongolia is 636–655 Ma (Jian *et al.* 2010a), 568 Ma in the Khantaishir area of western Mongolia (Gibsher *et al.* 2001) and 571 Ma in the Bayannur area of Western Mongolia (Khain *et al.* 2003). The formation age of the Toudaoqiao blueschists ranges over 511–516 Ma in the eastern Mongolian arc (Zhou *et al.* 2015; Liu *et al.* 2017), over 510–539 Ma for the Xinlin ophiolites, and is *c.* 630 Ma for the Gaxian ophiolites (Feng, 2015). Furthermore, Ge *et al.* (2005) and Wu *et al.* (2005b) dated post-collisional granites at 517–504 Ma and 494–480 Ma, respectively, marking the end of subduction beneath the Mongolian arc, in the north of Heilongjiang Province. The above data show that the Mongolian arc was activated before the Early Ordovician Period. As a result of this study, the Mante Aobao granite porphyry formed during the Late Ordovician Period (at *c.* 450–445 Ma), which is clearly later than the Mongolian arc, and hence are unrelated to that arc-building episode.

A lower Palaeozoic arc-related magmatic belt is also present along the Sonid Zuoqi to Xilinhot axis (with a magmatic age of 416–496 Ma) to the south of the Mante Aobao granite porphyry (Fig. 1b), most probably resulting from northwards subduction of the Paleo-Asian Ocean (Shi *et al.* 2004; Jian *et al.* 2008; Li *et al.* 2014c; Wang *et al.* 2016). Northwards subduction was recorded by the subduction-related diorite from the Hada pluton to the north of Siziwangqi with an age of 508 ± 10 Ma (Zhou *et al.* 2009), coeval with eruption of the Duobaoshan volcano. Arc magmas on the southern margin of Sonid Zuoqi yielded a SHRIMP

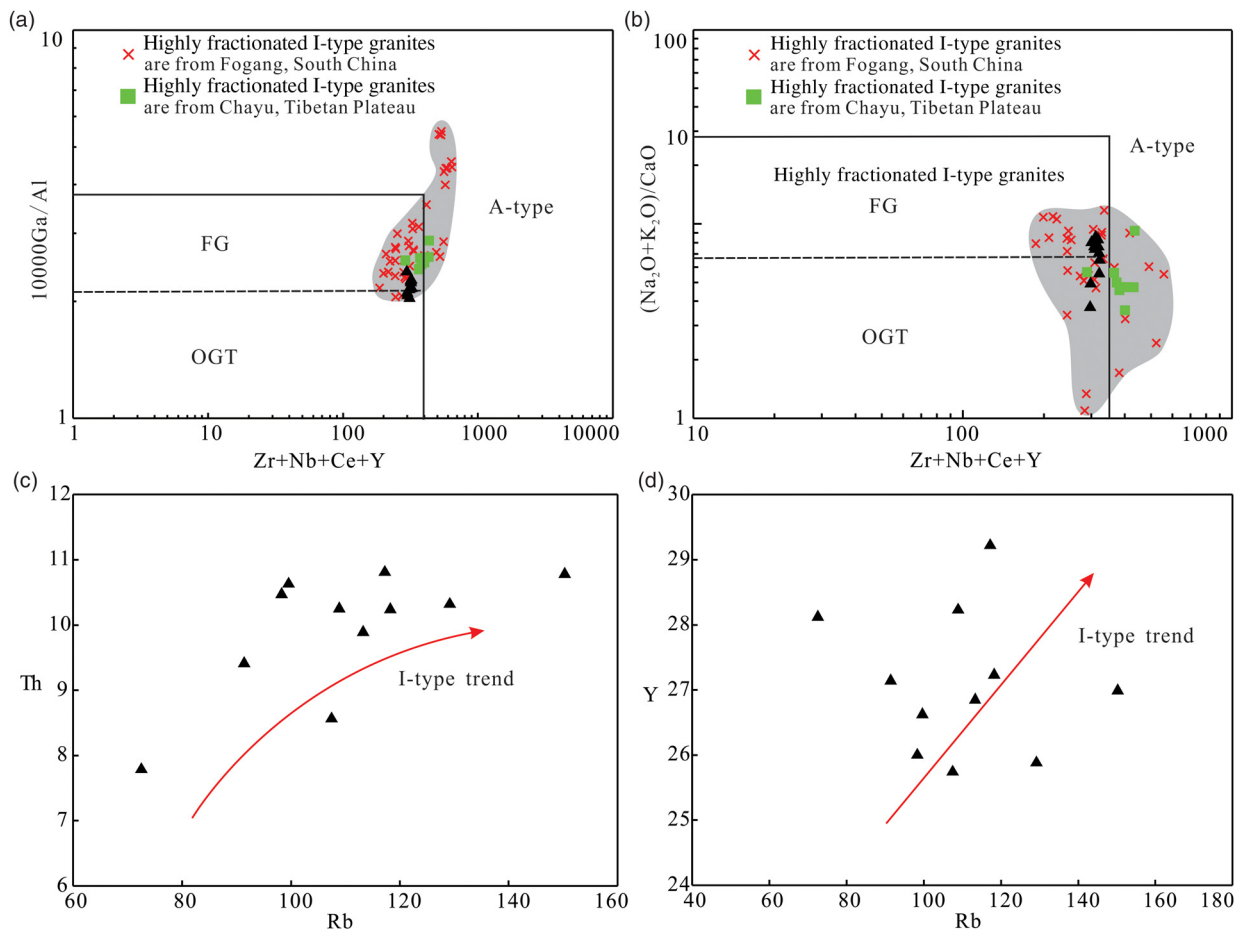


Fig. 7. (Colour online) Plots of (a) $10\,000 \times \text{Ga}/\text{Al}$ and (b) $(\text{K}_2\text{O} + \text{Na}_2\text{O})/\text{CaO}$ versus $(\text{Zr} + \text{Nb} + \text{Ce} + \text{Y})$ (Whalen *et al.* 1987), (c) Th versus Rb and (d) Y versus Rb (Chappell & White, 1992) for the Mante Aobao granite porphyry in East Ujimqin Banner. Additional highly fractionated I-type granite data are from Fogang, South China (Li *et al.* 2007) and Chayu, Tibetan Plateau (Zhu *et al.* 2009).

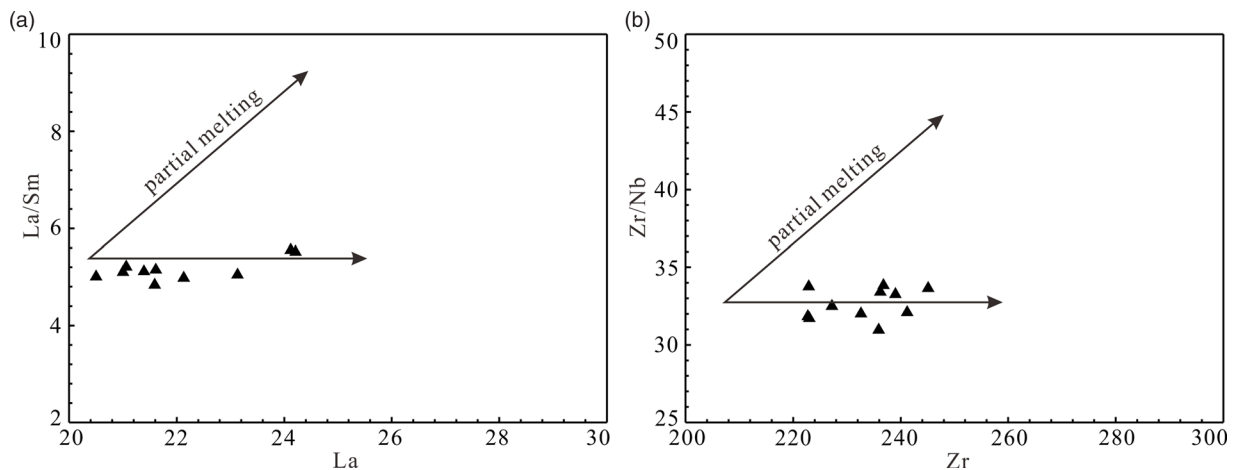


Fig. 8. (a) La/Sm versus La diagram and (b) Zr/Nb versus Zr diagram for the Mante Aobao granite porphyry in East Ujimqin Banner.

zircon U–Pb age of 490 ± 8 Ma, indicating that arc magmatism is also related to N-dipping subduction of the Paleo-Asian Ocean (Chen *et al.* 2001). The age of Xilin Gol magmatism is in line with SHRIMP zircon U–Pb ages of 464 ± 8 Ma and 479 ± 8 Ma from the Baiyinbaolidao adakitic tonalities at Sonid Zuoqi (Shi *et al.* 2005).

The data presented in this paper therefore show that the Mante Aobao granite porphyry formed during the same magmatic period

previously identified for the Sonid Zuoqi to Xilinhot axis (Shi *et al.* 2004, 2016; Zhao *et al.* 2012; Li *et al.* 2016; Yang *et al.* 2017, 2018). Furthermore, it has been suggested in previous studies (Cui *et al.* 2008; Wilhem *et al.* 2012; Zhao *et al.* 2012; Yang *et al.* 2014; Zhu *et al.* 2014; Li *et al.* 2016) that the lower Palaeozoic zone adjacent to our study area was related to an active continental margin. These studies have also indicated that the magmatic rocks, along with

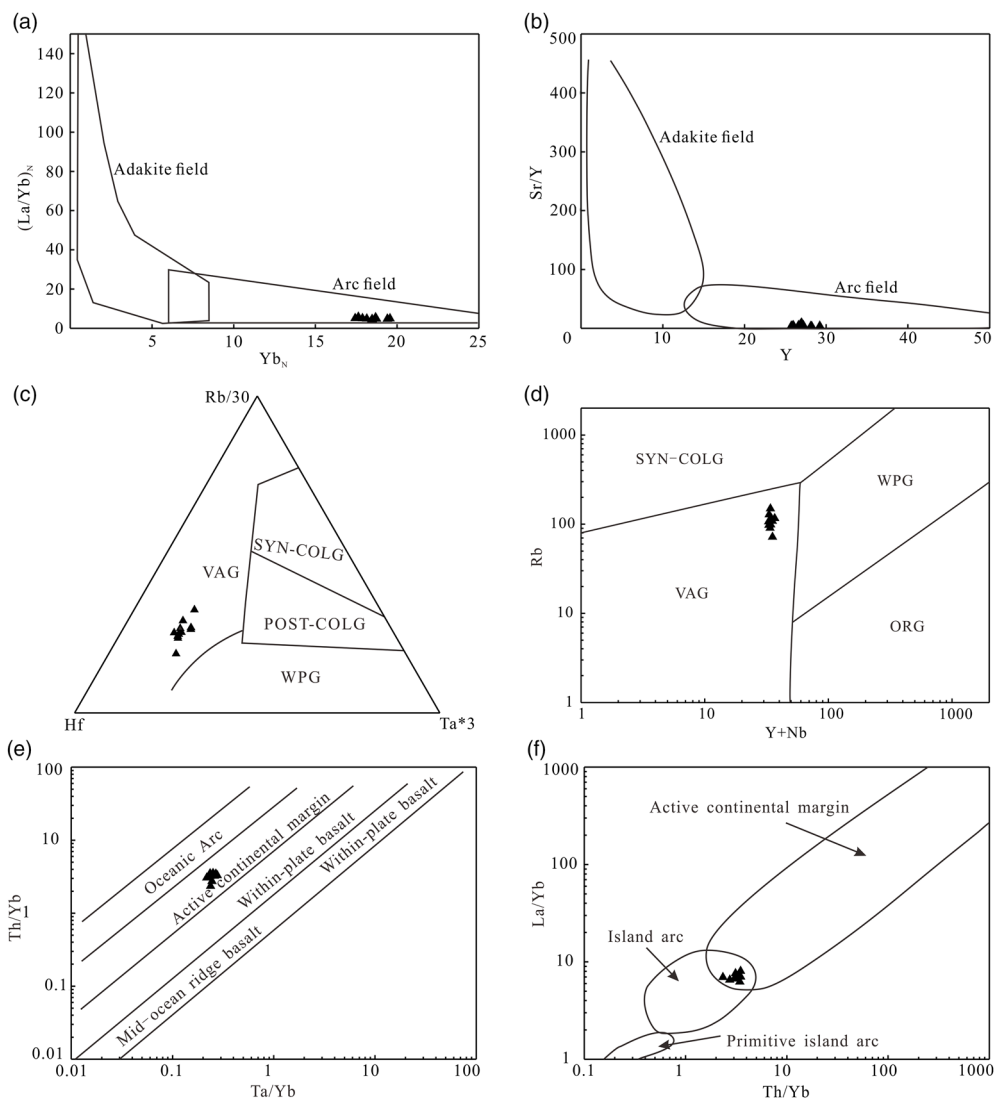


Fig. 9. Tectonic discrimination diagrams for the Mante Aobao granite porphyry in East Ujimqin Banner. (a) $(La/Yb)_N$ versus Yb_N (Defant & Drummond, 1990); (b) Sr/Y versus Y (Defant & Drummond, 1990); (c) $(Ta \times 3) - (Rb/30) - Hf$ triangular diagram (Harris *et al.* 1986); (d) Rb versus $Y+Nb$ (Pearce *et al.* 1984); (e) Th/Yb versus Ta/Yb (Gorton & Schandl, 2000); and (f) La/Yb versus Th/Yb (Condie, 1989). VAG – volcanic arc granites; ORG – ocean ridge granites; WPG – within-plate granites; SYN-COLG – syn-collisional granites; POST-COLG – post-collisional granites.

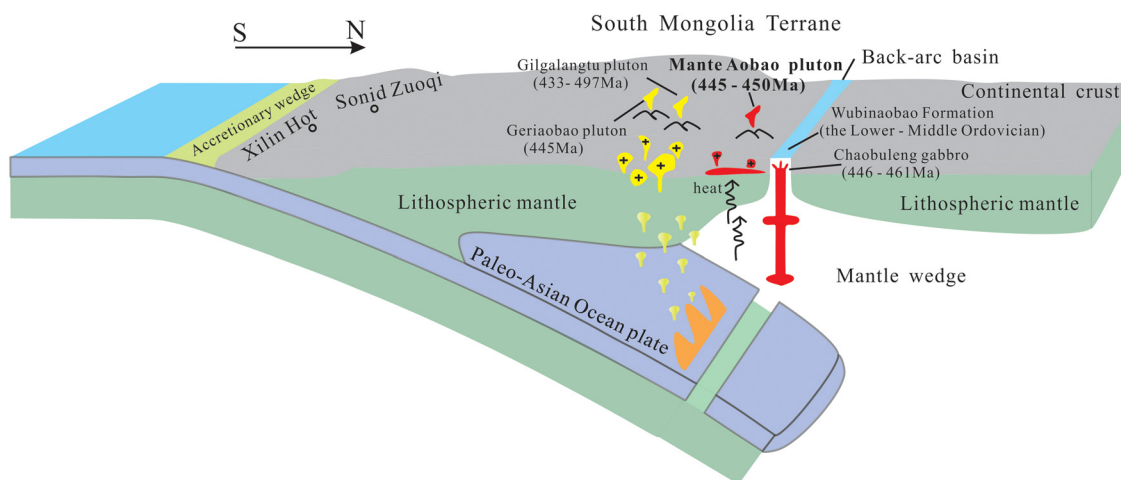


Fig. 10. (Colour online) Tectono-magmatic model for the Mante Aobao granite porphyry in East Ujimqin Banner, see text for details.

volcanic rocks of the Duobaoshan Formation that indicate an island arc to the south, constitute an arc-basin system (Cui *et al.* 2008; Zhao *et al.* 2012; Yang *et al.* 2014; Li *et al.* 2016). The Mante Aobao granite porphyry most likely formed by the northwards subduction of the Paleo-Asian Ocean during the early Palaeozoic Era. However, the lower Palaeozoic magmatic rocks in the Uliastai continental margin, including the Mante Aobao granite porphyry, are located some considerable distance from the Sonid Zuoqi to Xilinhot axis (Fig. 1b), and are separated by the Hegenshan ophiolite belt. Moreover, previous studies (Chen *et al.* 2000; Li *et al.* 2016; Shi *et al.* 2016; Wang *et al.* 2016) have not addressed the relation between the region's rocks and the Sonid Zuoqi to Xilinhot subduction zone. With regard to the tectonic evolution of the study area, Miao *et al.* (2008) considered that northwards subduction of the Paleo-Asian Ocean led to the formation of the Baolidao arc-related magmatic rocks in the Sonid Zuoqi area. Subsequently, the Hegenshan Ocean opened after generation of the Baolidao arc, and it was postulated this was due to the influence of slab rollback and back-arc extension. Furthermore, these authors suggested that the ocean basin closed during early–middle Permian time, thus forming the Hegenshan ophiolite belt. A similar scenario was proposed by Eizenhöfer *et al.* (2014), who used detrital zircon ages and Hf isotopes of the Palaeozoic strata in the Xing'an–Mongolian Orogenic Belt to suggest that the Mongolian arc collided along the Sonid Zuoqi to Xilinhot collision zone during the early Carboniferous Period. They further suggested that the subducted Paleo-Asian Ocean plate retreated and that subsequently the Mongolian arc and subduction belt separated again, forming the Hegenshan Ocean, and that this ocean closed during middle–late Permian time. A study of Ordovician–Permian sediments in the Chagan'aobao area to the north of the Hegenshan ophiolite belt by Xu *et al.* (2017) showed that such a shift in detrital zircon ages implies that the Sonid Zuoqi to Xilinhot collision zone was no longer a contributor of detritus during Carboniferous – early Permian time because of the opening of the 'Hegenshan Ocean', possibly induced by slab rollback of the subducting Paleo-Asian Ocean plate. The Dahate fore-arc basalt was identified by Li *et al.* (2018) in the western sector of the Diyanmiao Ophiolite (Fig. 1b), which suggests that the initial subduction of the oceanic plate and magmatism in the ocean–continent transition zone occurred when the Hegenshan Ocean existed during the early Carboniferous Period. Jian *et al.* (2012) dated the gabbro and granite in the 'Hegenshan ophiolites' at 354 Ma and 333 Ma, respectively. Later, Zhang *et al.* (2015b) similarly dated the ophiolites in the Erenhot area at 345–355 Ma. Although some controversy remains about the formation time and evolution of the Hegenshan Ocean, ocean basin opening can be dated to a time later than the formation of the Mante Aobao granite porphyry. To summarize, the Mante Aobao granite porphyry was most likely a part of the magmatic arc formed by northwards subduction of the early Palaeozoic Paleo-Asian Ocean along the Sonid Zuoqi to Xilinhot axis. It may therefore represent part of the magmatic island-arc or back-arc basin (Li *et al.* 2016); its distance from the subduction zone could be explained by its separation from the main body of the arc during a later period characterized by the opening of the Hegenshan Ocean. Afterwards, the gradual closure of the Hegenshan Ocean resulted in the current geographic location of the Mante Aobao granite porphyry and explains why it was separated from the Sonid Zuoqi to Xilinhot subduction–collision axis.

In conclusion, a Late Ordovician tectono-magmatic model based on data from the Mante Aobao granite porphyry can be

summarized as follows (Fig. 10). During the Late Ordovician Period, the Paleo-Asian oceanic plate subducted northwards beneath the South Mongolian micro-continent along the Sonid Zuoqi to Xilinhot axis. Subsequently, the subducting oceanic slab broke off and sank (Jian *et al.* 2008; Li *et al.* 2016), which induced lithospheric thinning and asthenospheric mantle upwelling, forming a back-arc basin in the East Ujimiqin Banner area. This can be confirmed by the presence of an Upper Ordovician gabbro, which exhibits the geochemical characteristics of both mid-ocean-ridge basalt (MORB) and subduction-related island-arc basalt (IAB) (Li *et al.* 2016). The distribution and rock assemblages characteristic of the Lower–Middle Ordovician Duobaoshan and Wubinaobao formations that crop out near the research area are also consistent with the sedimentary features of a back-arc basin (Zhu, 1986; Yu *et al.* 1996; Peng *et al.* 1999; Xie, 2013; Wu *et al.* 2015b; Li *et al.* 2016). The upwelling of asthenospheric mantle provided sufficient heat for the partial melting of juvenile crust at the back of the active continental margin, generating highly fractionated I-type granites.

6. Conclusions

- (1) The Mante Aobao granite porphyry formed at 450–445 Ma during the Late Ordovician Period, and geochemical data indicate that it is a highly fractionated I-type granite.
- (2) Combined with the geochemical characteristics of the pluton, the zircon Hf isotope signatures (positive $\varepsilon_{\text{Hf}}(t)$ values with young Hf model ages) indicate that it most likely originated from the partial melting of Neoproterozoic juvenile crust, with the uprise of mantle-derived magmas as a result of crustal thinning providing the heat for crustal melting. This melt subsequently underwent fractional crystallization during the uprise of the Mante Aobao pluton.
- (3) Several lines of evidence indicate that the Mante Aobao granite porphyry was emplaced at an active continental margin that was related to the northwards subduction of the Paleo-Asian Plate beneath the South Mongolian Terrane along the Sonid Zuoqi to Xilinhot axis.

Acknowledgements. This work was supported by the China Geological Survey (12120113089000) and Integration and Processing of Geological Survey Data (DD20190429). We are grateful to Professor Brian Windley, Dr Songfeng Liu and Shengdong Wang for constructive discussions. We also extend our thanks to the editor Dr Kathryn Goodenough for her thoughtful comments and editorial handling of the manuscript and to two anonymous reviewers for their useful suggestions that have led to significant improvements in our manuscript.

References

- Andersen T (2002) Correction of common lead in U–Pb analyses that do not report ^{204}Pb . *Chemical Geology* **192**, 59–79.
- Badarch G, Cunningham WD and Windley BF (2002) A new terrane subdivision for Mongolia: implications for the Phanerozoic crustal growth of Central Asia. *Journal of Asian Earth Sciences* **21**, 87–110.
- Baker MB, Hirschmann MM, Ghiorso MS and Stolper EM (1995) Compositions of near-solidus peridotite melts from experiments and thermodynamic calculations. *Nature* **375**, 308–11.
- Baxter S and Feely M (2002) Magma mixing and mingling textures in granitoids: examples from the Galway Granite, Connemara, Ireland. *Mineralogy and Petrology* **76**, 63–74.
- Blichert-Toft J and Albarede F (1997) The Lu–Hf isotope geochemistry of chondrites and the evolution of the mantle–crust system. *Earth and Planetary Science Letters* **148**, 243–58.

- Bonin B** (2007) A-type granites and related rocks: evolution of a concept, problems and prospects. *Lithos* **97**, 1–29.
- Chappell BW** (1999) Aluminium saturation in I- and S-type granites and the characterization of fractionated haplogranites. *Lithos* **46**, 535–51.
- Chappell BW and White AJR** (1974) Two contrasting granite types. *Pacific Geology* **8**, 173–74.
- Chappell BW and White AJR** (1992) I- and S-type granites in the Lachlan Fold Belt. *Transactions of the Royal Society of Edinburgh: Earth Sciences* **83**, 1–26.
- Chappell BW and White AJR** (2001) Two contrasting granite types: 25 years later. *Australian Journal of Earth Sciences* **48**, 489–99.
- Chen B, Jahn BM and Tian W** (2009) Evolution of the Solonker suture zone: constraints from zircon U-Pb ages, Hf isotopic ratios and whole-rock Nd-Sr isotope compositions of subduction and collision-related magmas and fore-arc sediments. *Journal of Asian Earth Sciences* **34**, 245–57.
- Chen B, Jahn BM, Wilde SA and Xu B** (2000) Two contrasting Paleozoic magmatic belts in northern Inner Mongolia, China: petrogenesis and tectonic implications. *Tectonophysics* **328**, 157–82.
- Chen B and Xu B** (1996) The main characteristics and tectonic implications of two kinds of Paleozoic granitoids in Sunidzuqi, Central Inner Mongolia. *Acta Petrologica Sinica* **12**, 546–61 (in Chinese with English abstract).
- Chen B, Zhao GC and Wilde SA** (2001) Subduction- and collision-related granitoids from southern Sonidzuqi, Inner Mongolia: isotopic ages and tectonic implications. *Geological Review* **47**, 361–7 (in Chinese with English abstract).
- Chen C, Zhang ZC, Guo ZJ, Li JF, Feng ZS and Tang WH** (2012) Geochronology, geochemistry and its geological significance of the Permian Mandala mafic rocks in Damaoqi, Inner Mongolia. *Science China Earth Sciences* **55**, 39–52 (in Chinese).
- Condie KC** (1989) Geochemical changes in basalts and andesites across the Archean-Proterozoic boundary: identification and significance. *Lithos* **23**, 1–18.
- Corfu F, Hanchar JM, Hoskin PWO and Kinny P** (2003) Atlas of zircon textures. *Reviews in Mineralogy & Geochemistry* **53**, 469–95.
- Cui G, Wang JY, Zhang JX and Cui G** (2008) U-Pb SHRIMP dating of zircons from Duobaoshan granodiorite in Heilongjiang and its geological significance. *Global Geology* **27**, 387–94 (in Chinese with English abstract).
- Defant MJ and Drummond MS** (1990) Derivation of some modern arc magmas by melting of young subducted lithosphere. *Nature* **347**, 662–65.
- Eizenhöfer PR, Zhao GC, Sun M, Zhang J, Han YG and Hou WZ** (2015) Geochronological and Hf isotopic variability of detrital zircons in Paleozoic strata across the accretionary collision zone between the north China craton and Mongolian arcs and tectonic implications. *Geological Society of America Bulletin* **65**, 487–508.
- Eizenhöfer PR, Zhao GC, Zhang J and Sun M** (2014) Final closure of the Paleo-Asian Ocean along the Solonker Suture Zone: constraints from geochronological and geochemical data of Permian volcanic and sedimentary rocks. *Tectonics* **33**, 441–63.
- Feng ZQ** (2015) Paleozoic tectonic-magmatic evolution of Northern Great Hinggan Mountains. PhD thesis, College of Earth Sciences, Jinlin University, Changchun, China (in Chinese with English abstract). Published thesis.
- Fisher CM, Vervoort JD and Hanchar JM** (2014) Guidelines for reporting zircon Hf isotopic data by LA-MC-ICPMS and potential pitfalls in the interpretation of these data. *Chemical Geology* **363**, 125–33.
- Frost BR, Barnes CG, Collins WJ, Arculus RJ, Ellis DJ and Frost CD** (2001) A geochemical classification for granitic rocks. *Journal of Petrology* **47**, 2033–48.
- Ge MC, Zhou WX, Yu Y, Sun JJ, Bao JQ and Wang SH** (2011) Dissolution and supracrustal rocks dating of Xilin Gol Complex, Inner Mongolia, China. *Frontiers of Earth Science* **18**, 182–95 (in Chinese with English abstract).
- Ge WC, Wu FY, Zhou CY and Rahman AA** (2005) The age of Tahe granites of northern Greater Khingan Mountains and its constraints on the tectonic evolution of Erguna massif. *Chinese Science Bulletin* **50**, 1239–47 (in Chinese).
- Gibsher AS, Khain EV, Kotov AB, Salnikova E, Kozakov KI, Kovach VP, Yakovleva SZ and Fedoseenko AM** (2001) Late Vendian age of the Han-Taishiri ophiolitic complex in western Mongolia. *Russian Geology Geophysics* **42**, 1110–17.
- Gorton MP and Schandl ES** (2000) From continents to island arcs: a geochemical index of tectonic setting for arc-related and within-plate felsic to intermediate volcanic rocks. *Canadian Mineralogist* **38**, 1065–73.
- Griffin WL, Pearson NJ, Belousova E, Jackson SE, van Acherbergh E, O'Reilly SY and Shee SR** (2000) The Hf isotope composition of cratonic mantle: LAM-MC-ICPMS analysis of zircon megacrysts in kimberlites. *Geochimica et Cosmochimica Acta* **64**, 133–47.
- Guo F, Fan WM, Li CW, Miao LC and Zhao L** (2009) Early Paleozoic subduction of the Paleo-Asian Ocean: Geochronological and geochemical evidence from the Dashizhai basalts, Inner Mongolia. *Science China Earth Sciences* **52**, 940–51 (in Chinese with English abstract).
- Harris NBW, Pearce JA and Tindle AG** (1986) Geochemical characteristic of collision-zone magmatism. In *Collision Tectonics* (eds MP Coward and AC Ries), pp. 67–81. Geological Society of London, Special Publication no. 19.
- Hibbard MJ** (1991) Textural anatomy of twelve magma mixed granitoid systems. In *Enclaves and Granite Petrology* (eds J Didier and B Barbarin), pp. 431–44. Elsevier: Amsterdam, Netherlands, *Developments in Petrology* no. 13.
- Hu ZC, Liu YS, Gao S, Liu WG, Yang L, Zhang W, Tong XR, Lin L, Zong KQ, Li M, Chen HH, Zhou L and Yang L** (2012) Improved in situ Hf isotope ratio analysis of zircon using newly designed X skimmer cone and Jet sample cone in combination with the addition of nitrogen by laser ablation multiple collector ICP-MS. *Journal of Analytical Atomic Spectrometry* **27**, 1391–99.
- Irvine TN and Baragar WRA** (1971) A guide to the chemical classification of the common volcanic rocks. *Canadian Journal of Earth Sciences* **8**, 523–48.
- Jahn BM, Natal'in B, Windley B and Dobretsov N** (2004) Phanerozoic continental growth in Central Asia. *Journal of Asian Earth Sciences* **23**, 599–603.
- Jahn BM, Wu FY and Chen B** (2000) Granitoids of the Central Asian Orogenic Belt and continental growth in the Phanerozoic. *Transactions of the Royal Society of Edinburgh: Earth Sciences* **91**, 181–93.
- Jian P, Kröner A, Windley BF, Shi YR, Zhang FQ, Miao LC, Tomurhuu D, Zhang W and Liu DY** (2010a) Zircon ages of the Bayankhongor ophiolite mélange and associated rocks: time constraints on Neoproterozoic to Cambrian accretionary and collisional orogenesis in central Mongolia. *Precambrian Research* **177**, 162–80.
- Jian P, Kröner A, Windley BF, Shi YY, Zhang W, Zhang LQ and Yang WR** (2012) Carboniferous and Cretaceous mafic-ultramafic massifs in Inner Mongolia (China): a SHRIMP zircon and geochemical study of the previously presumed integral “Hegenshan Ophiolite”. *Lithos* **142**, 48–66.
- Jian P, Liu DY, Kröner A, Windley BF, Shi YR, Zhang FQ, Shi GH, Miao LC, Zhang W, Zhang Q, Zhang LQ and Ren JS** (2008) Time scale of an early to mid-Paleozoic orogenic cycle of the long-lived Central Asian Orogenic Belt, Inner Mongolia of China: implications for continental growth. *Lithos* **101**, 233–59.
- Jian P, Liu DY, Kröner A, Windley BF, Shi YR, Zhang W, Zhang FQ, Miao LC, Zhang LQ and Tomurhuu D** (2010b) Evolution of a Permian intraoceanic arc-trench system in the Solonker suture zone, Central Asian Orogenic Belt, China and Mongolia. *Lithos* **118**, 169–90.
- Jong KD, Xiao WJ, Windley BF, Masago H and Lo CH** (2006) Ordovician $^{40}\text{Ar}/^{39}\text{Ar}$ phengite ages from the blueschist-facies Ondor Sum subduction-accretion complex (Inner Mongolia) and implications for the early Paleozoic history of continental blocks in China and adjacent area. *American Journal of Science* **306**, 799–845.
- Khain EV, Bibikova EV, Salnikova EB, Kröner A, Gibsher AS, Didenko A, Degtyarev KE and Fedotova A** (2003) The Palaeo-Asian Ocean in the Neoproterozoic and early Palaeozoic: new geochronologic data and palaeotectonic reconstructions. *Precambrian Research* **122**, 329–58.
- Kovalenko VI, Yarmolyuk VV, Kovach VP, Kotov AB, Kozakov IK, Salnikova EB and Larin AM** (2004) Isotope provinces, mechanisms of generation and sources of the continental crust in the Central Asian Mobile Belt: geological and isotopic evidence. *Journal of Asian Earth Sciences* **23**, 605–27.
- Li HY, Zhou ZG, Li PJ, Zhang D, Liu CF, Zhao XQ, Chen LZ, Gu CN, Lin TT and Hu MM** (2016) Ordovician intrusive rocks from the eastern Central Asian Orogenic Belt in Northeast China: chronology and implications for bidirectional subduction of the early Paleozoic Palaeo-Asian Ocean. *International Geology Review* **10**, 1175–95.

- Li JY (2006) Permian geodynamic setting of Northeast China and adjacent regions: closure of the Paleo-Asian Ocean and subduction of the Paleo-Pacific plate. *Journal of Asian Earth Sciences* **26**, 207–24.
- Li JY, Gao LM and Sun GH (2007) Shuangjingzi middle Triassic syn-collisional crust-derived granite in the east Inner Mongolia and its contrast on the timing of collision between Siberian and Sino–Korean Paleo-Plates. *Acta Petrologica Sinica* **23**, 565–82 (in Chinese with English abstract).
- Li K, Zhang ZC, Feng ZS, Li JF, Tang WH and Luo ZW (2014a) Zircon SHRIMP U–Pb dating and its geological significance of the late-Carboniferous to early-Permian volcanic rocks in Bayanwula area, the central of Inner Mongolia. *Acta Petrologica Sinica* **30**, 2041–54 (in Chinese with English abstract).
- Li S, Wilde SA, Wang T, Xiao WJ and Guo QQ (2014b) Latest early Permian granitic magmatism in southern Inner Mongolia, China: implications for the tectonic evolution of the southeastern Central Asian Orogenic Belt. *Gondwana Research* **29**, 168–80.
- Li XH, Li ZX, Li WX, Liu Y, Yuan C, Wei GJ and Qi CS (2007) U–Pb zircon, geochemical and Sr–Nd–Hf isotopic constraints on age and origin of Jurassic I- and A-type granites from central Guangdong, SE China: a major igneous event in response to foundering of a subducted flat-slab? *Lithos* **96**, 186–204.
- Li YJ, Wang JF, Wang GH, Li HY and Dong PP (2018) Discovery and significance of the Dahate fore-arc basalts from the Diyanmiao ophiolite in Inner Mongolia. *Acta Petrologica Sinica* **34**, 469–82 (in Chinese with English abstract).
- Li YL, Zhou HW, Brouwer FM, Wijbrans JR, Zhong ZQ and Liu HF (2011) Tectonic significance of the Xilin Gol Complex, Inner Mongolia, China: petrological, geochemical and U–Pb zircon age constraints. *Journal of Asian Earth Sciences* **42**, 1018–29.
- Li YL, Zhou HW, Brouwer FM, Xiao WJ, Wijbrans JR and Zhong ZQ (2014c) Early Paleozoic to middle Triassic bivertent accretion in the Central Asian Orogenic Belt: insights from zircon U–Pb dating of ductile shear zones in central Inner Mongolia, China. *Lithos* **205**, 84–111.
- Liu DY, Jian P, Zhang Q, Zhang FQ, Shi YR, Shi GH, Zhang LQ and Tao H (2003) Shrimp dating of adakites in the Tulingkai ophiolite, Inner Mongolia: evidence for the early Paleozoic subduction. *Acta Petrologica Sinica* **77**, 317–27 (in Chinese with English abstract).
- Liu JF, Li JY, Chi XG, Zhao Z, Hu ZC and Feng QW (2012) Petrogenesis of middle Triassic post-collisional granite from Jiefangyingzi area, southeast Inner Mongolia: Constraint on the Triassic tectonic evolution of the north margin of the Sino–Korean paleoplate. *Journal of Asian Earth Sciences* **60**, 147–59.
- Liu Y, Gao S, Hu Z, Gao C, Zong K and Wang D (2010) Continental and oceanic crust recycling-induced melt-peridotite interactions in the Trans-North China Orogen: U–Pb dating, Hf isotopes and trace elements in zircons from mantle xenoliths. *Journal Petrology* **51**, 537–71.
- Liu Y, Hu Z, Gao S, Nther GU, Xu J, Gao C and Chen H (2008) In situ analysis of major and trace elements of anhydrous minerals by LA-ICP-MS without applying an internal standard. *Chemical Geology* **257**, 34–43.
- Liu YJ, Li WM, Feng ZQ, Wen QB, Neubauer F and Liang C (2017) A review of the Paleozoic tectonics in the eastern part of Central Asian Orogenic Belt. *Gondwana Research* **43**, 123–48.
- Ludwig KR (2003) *User's manual for Isoplot/EX, version 3.0: A geochronological toolkit for Microsoft Excel*. Berkeley: Berkeley Geochronology Center Special Publication.
- Ma XH, Chen CJ, Zhao JX, Qiao SL and Zhou ZH (2019) Late Permian intermediate and felsic intrusions in the eastern Central Asian Orogenic Belt: final-stage magmatic record of Paleo-Asian Oceanic subduction? *Lithos* **326**, 265–78.
- Miao LC, Fan WM, Liu DY, Zhang FQ, Shi YR and Guo F (2008) Geochronology and geochemistry of the Hegenshan Ophiolitic complex: implications for late-stage tectonic evolution of the Inner Mongolia-Daxinganling Orogenic Belt, China. *Journal of Asian Earth Sciences* **32**, 348–70.
- Miao LC, Zhang FQ, Fan WM and Liu DY (2007) Phanerozoic evolution of the Inner Mongolia-Daxinganling orogenic belt in North China: Constraints from geochronology of ophiolites and associated formations. In *Mesozoic Sub-Continental Lithospheric Thinning Under Eastern Asia* (eds M-G Zhai, BF Windley, TM Kusky and QR Meng), pp. 223–37. Geological Society of London, Special Publication no. 280.
- Middlemost EAK (1994) Naming materials in the magma/igneous rock system. *Earth Science Reviews* **37**, 215–24.
- Pearce JA, Harris NBW and Tindle AG (1984) Trace element discrimination diagrams for the tectonic interpretation of granitic rocks. *Journal of Petrology* **25**, 956–83.
- Peccerillo A and Taylor SR (1976) Geochemistry of Eocene calc-alkaline volcanic rocks from the Kastamonu area, northern Turkey. *Mineralogy and Petrology* **58**, 63–81.
- Peng YM, Pan GT and Luo JN (1999) Volcanic-sedimentary feature of back-arc basin. *Sedimentary Facies and Paleogeography* **19**, 65–72 (in Chinese with English abstract).
- Perugini D and Poli G (2012) The mixing of magmas in plutonic and volcanic environments: Analogies and differences. *Lithos* **153**, 261–77.
- Rickwood PC (1989) Boundary lines within petrologic diagrams which use oxides of major and minor elements. *Lithos* **22**, 247–63.
- Robinson PT, Zhou MF, Hu XF, Reynolds P, Bai W and Yang JS (1999) Geochemical constraints on the origin of the Hegenshan ophiolite, Inner Mongolia, China. *Journal of Asian Earth Sciences* **17**, 423–42.
- Scherer E, Munker C and Mezger K (2001) Calibration of the lutetium-hafnium clock. *Science* **293**, 683–87.
- Sengör AMC and Natal'in BA (1996) Turkic-type orogeny and its role in the making of the continental crust. *Annual Review Earth and Planetary Sciences* **24**, 263–337.
- Shi YR, Liu DY, Jian P, Zhang Q, Zhang FQ, Miao LC, Shi GH, Zhang LQ and Tao H (2005) The petrogenesis and SHRIMP dating of the Baiyinbaolidao adakitic rocks in southern Suzuqi, Inner Mongolia. *Acta Petrologica Sinica* **21**, 143–50 (in Chinese with English abstract).
- Shi GH, Liu DY, Zhang FQ, Jian P, Miao LC, Shi YR and Tao H (2003) SHRIMP U–Pb zircon geochronology and its implications on the Xilin Gol Complex, Inner Mongolia, China and its implications. *Chinese Science Bulletin* **48**, 2742–48 (in Chinese with English abstract).
- Shi GH, Miao LC, Zhang FQ, Jian P, Fan WM and Liu DY (2004) The age and its district tectonic implications on the Xilinhaote A-type granites, Inner Mongolia. *Chinese Science Bulletin* **49**, 384–89 (in Chinese with English abstract).
- Shi GZ, Faure M, Xu B, Zhao P and Chen Y (2013) Structural and kinematic analysis of the early Paleozoic Ondor Sum–Hongqi mélange belt, eastern part of the Altaids (CAOB) in Inner Mongolia, China. *Journal of Asian Earth Sciences* **66**, 123–39.
- Shi YR, Jian P, Kröner A, Li LL, Liu C and Zhang W (2016) Zircon ages and Hf isotopic compositions of Ordovician and Carboniferous granitoids from central Inner Mongolia and their significance for early and late Paleozoic evolution of the Central Asian Orogenic Belt. *Journal of Asian Earth Sciences*, **117**, 153–69.
- Shi YR, Liu C, Deng JF and Jian P (2014) Geochronological frame of granitoids from Central Inner Mongolia and its tectonomagmatic evolution. *Acta Petrologica Sinica* **30**, 3155–71 (in Chinese with English abstract).
- Shi YR, Liu DY, Jian P, Zhang Q, Zhang FQ, Miao LC, Shi GH, Zhang LQ and Tao H (2004) The petrogenesis and SHRIMP dating of the Baiyinbaolidao adakitic rocks in southern Suzuqi, Inner Mongolia. *Acta Petrologica Sinica* **21**, 143–50 (in Chinese with English abstract).
- Sisson TW, Ratajeski K, Hankins WB and Glazner AF (2005) Voluminous granitic magmas from common basaltic sources. *Contributions to Mineralogy and Petrology* **148**, 635–61.
- Su YZ (1996) Paleozoic stratigraphy of Nei Mongol Grass stratigraphical province. *Jilin Geology* **15**, 41–54 (in Chinese with English abstract).
- Sui ZM, Ge WC, Wu FY, Zhang JH, Xu XC and Cheng RY (2007) Zircon U–Pb ages, geochemistry and its petrogenesis of Jurassic granites in northeastern part of the Da Hinggan Mountains. *Acta Petrologica Sinica* **23**, 461–80 (in Chinese with English abstract).
- Sun SS and McDonough WF (1989) Chemical and isotopic systematics of oceanic basalts: Implications for mantle composition and processes. In *Magmatism in the Ocean Basin* (eds AD Saunders and MJ Norry), pp. 313–45. Geological Society of London, Special Publication no. 42.
- Tang KD (1990) Tectonic development of Paleozoic foldbelts at the north margin of the Sino–Korean Craton. *Tectonics* **9**, 249–60.
- Tang KD (1992) *Tectonic Evolution and Minerogenetic Regularities of the Fold Belt along the Northern Margins of Sino-Korean Plate*. Publishing House of Beijing University, Beijing, pp. 108–111 (in Chinese).

- Tang KD and Shao JA** (1996) Some characteristics of ophiolites and ancient ocean evolution in paleoasia oceanic area. In *Proceedings of Symposium on Ophiolites and Geodynamics*, pp. 108–111. Geological Publishing House, Beijing, 108–111 (in Chinese with English abstract).
- Tang KD and Yan ZY** (2007) Regional metamorphism and tectonic evolution of the Inner Mongolian suture zone. *Journal of Metamorphic Geology* **11**, 511–22.
- Tang KD and Zhang YP** (1991) Tectonic evolution of Inner Mongolia. In *Tectonic Evolution of the Southern Margin of the Paleo-Asian Composite Megasuture* (eds XC Xiao and YQ Tang), pp. 30–53. Scientific and Technical Publishing House, Beijing, no. 2 (in Chinese).
- Tao JX, Xu LQ, He F and Su MR** (2005) Petrological evidence for subduction of the early Paleozoic oceanic crust in Bart-Obo, Inner Mongolia. *Geological Survey and Research* **28**, 1–8 (in Chinese with English abstract).
- Taylor SR and McLennan SM** (1985) *The Continental Crust: Its Composition and Evolution*. Blackwell Publishing, Oxford, pp. 312.
- Tong Y, Hong DW, Wang T, Shi JX, Zhang JJ and Zeng T** (2010) Spatial and temporal distribution of granitoids in the middle segment of the Sino-Mongolian Border and its tectonic and metallogenic implications. *Acta Petrologica Sinica* **31**, 395–412 (in Chinese with English abstract).
- Valley JW, Lackey JS, Cavosie AJ, Clechenko CC, Spicuzza MJ, Basei MAS, Bindeman IN, Ferreira VP, Sial AN, King EM, Peck WH, Sinha AK and Wei CS** (2005) 4.4 billion years of crustal maturation: oxygen isotope ratios of magmatic zircon. *Contributions to Mineralogy and Petrology* **150**, 561–80.
- Wan YS, Liu DY, Dong CY and Yin XY** (2011) SHRIMP zircon dating of meta-sedimentary rock from the Qinling Group in the north of Xixia, North Qinling Orogenic Belt: Constraints on complex histories of source region and timing of deposition and metamorphism. *Acta Petrologica Sinica* **27**, 1172–78 (in Chinese with English abstract).
- Wang Q and Liu XY** (1986) Paleoplate tectonics between Cathaysia and Angaraland in Inner Mongolia of China. *Tectonics* **5**, 1073–88.
- Wang SQ, Xin HT, Hu XJ, Zhang Y, Zhao HL, Geng JZ, Yang ZL, Teng HJ and Li YF** (2016) Geochronology, geochemistry and geological significance of early Paleozoic Wulanaobaotu intrusive rocks, Inner Mongolia. *Earth Science: Journal of China University of Geosciences* **41**, 555–69 (in Chinese with English abstract).
- Wang WQ, Xu ZY, Liu ZH, Zhao QY and Jiang XJ** (2013) Early-Middle Permian tectonic evolution of the central-northern margin of the North China Craton: constraints from zircon U-Pb ages and geochemistry of the granitoids. *Acta Petrologica Sinica* **29**, 2987–3003 (in Chinese with English abstract with English abstract).
- Wang YJ and Fan ZY** (1997) Discovery of Permian radiolarians in ophiolite belt on Northern side of Xar Moron river, Inner Mongolia, and its geological significance. *Acta Petrologica Sinica* **36**, 58–69 (in Chinese with English abstract).
- Watson EB and Harrison TM** (1983) Zircon saturation revisited: temperature and composition effect in a variety of crustal magmas types. *Earth and Planetary Science Letters* **64**, 295–304.
- Whalen JB, Currie KL and Chappell BW** (1987) A-type granites: geochemical characteristics, discrimination and petrogenesis. *Contributions to Mineralogy and Petrology* **95**, 407–19.
- Wilde SA** (2015) Final amalgamation of the Central Asian Orogenic Belt in NE China: Paleo-Asian Ocean closure versus Paleo-Pacific plate subduction: a review of the evidence. *Tectonophysics* **666**, 345–62.
- Wilde SA and Zhou JB** (2015) The late Paleozoic to Mesozoic evolution of the eastern margin of the Central Asian Orogenic Belt in China. *Journal of Asian Earth Sciences* **113**, 909–21.
- Wilhem C, Windley BF and Stampfli GM** (2012) The Altaids of Central Asia: A tectonic and evolutionary innovative review. *Earth Science Reviews* **113**, 303–41.
- Windley BF, Alexeiev D, Xiao WJ, Kröner A and Badarch G** (2007) Tectonic models for accretion of the Central Asian Orogenic Belt. *Journal of Geological Society of London* **164**, 31–47.
- Wu C, Liu CF, Zhu Y, Zhou ZG, Jiang T, Liu WC, Li HY, Wu C and Ye BY** (2015a) Early Paleozoic magmatic history of central Inner Mongolia, China: implications for the tectonic evolution of the southeast Central Asian Orogenic Belt. *International Journal of Earth Science* **105**, 1307–27.
- Wu FY, Jahn BM, Lo CH, Yui TF, Lin Q, Ge WC and Sun DY** (2003) Highly fractionated-type granites in NE China (II): isotopic geochemistry and implications for crustal growth in the Phanerozoic. *Lithos* **67**, 191–204.
- Wu FY, Jahn BM, Wilde SA and Sun DY** (2000) Phanerozoic continental crustal growth: Sr-Nd isotopic evidence from the granites in northeastern China. *Tectonophysics* **328**, 87–113.
- Wu FY, Li XH, Zheng YF and Gao S** (2007) Lu-Hf isotopic systematics and their applications in petrology. *Acta Petrologica Sinica* **23**, 185–220 (in Chinese with English abstract).
- Wu FY, Sun DY, Ge WC, Zhang YB, Grant ML, Wilde SA and Jahn BM** (2011) Geochronology of the Phanerozoic granitoids in northeastern China. *Journal of Asian Earth Sciences* **41**, 1–30.
- Wu FY, Sun DY and Lin Q** (1999) Petrogenesis of the Phanerozoic granites and crustal growth in Northeast China. *Acta Petrologica Sinica* **15**, 181–9 (in Chinese with English abstract).
- Wu FY, Yang JH, Wilde SA and Zhang XO** (2005a) Geochronology, petrogenesis and tectonic implications of Jurassic granites in the Liaodong Peninsula, NE China. *Chemical Geology* **221**, 127–56.
- Wu G, Chen YC, Sun FY, Liu J, Wang GR and Xu B** (2015b) Geochronology, geochemistry, and Sr-Nd-Hf isotopes of the early Paleozoic igneous rocks in the Duobaoshan area, NE China, and their geological significance. *Journal of Asian Earth Sciences* **97**, 229–50.
- Wu G, Sun FY, Zhao CS, Li ZT, Zhao AL, Pang QB and Li GY** (2005b) Discovery of early Paleozoic post-collision granites in the northern Ergun Massif and its geological significance. *Chinese Science Bulletin* **50**, 2278–88 (in Chinese with English abstract).
- Wu YB and Zheng YF** (2004) Genetic of zircon and its constraints on interpretation of U-Pb Age. *Chinese Science Bulletin* **49**, 1589–604 (in Chinese with English abstract).
- Wyborn D, Chappell BW and James M** (2001) Examples of convective fractionation in high temperature granites from the Lachlan Fold Belt. *Australian Journal of Earth Science* **48**, 531–41.
- Xiao WJ, Windley BF, Hao J and Zhai MG** (2003) Accretion leading to collision and the Permian Solonker suture, Inner Mongolia, China: termination of the Central Asian Orogenic Belt. *Tectonics* **22**, 1069–88.
- Xiao WJ, Zhang LC, Qin KZ, Sun S and Li JY** (2004) Paleozoic accretionary and collisional tectonics of the eastern Tianshan (China): implications for the continental growth of Central Asia. *American Journal of Science* **304**, 370–95.
- Xie LZ** (2013) Geochemical feature and tectonic evolution in eastern Duobaoshan, Heilongjiang. *Science and Technology of West China* **12**, 1–10 (in Chinese with English abstract).
- Xin HT, Teng XJ and Cheng YH** (2011) Stratigraphic subdivision and isotope geochronology study on the Baoligaomiao Formation in the East Ujimqin County, Inner Mongolia. *Geological Survey and Research* **34**, 1–9 (in Chinese with English abstract).
- Xu B, Charvet J, Chen Y, Zhao P and Shi GZ** (2013) Middle Paleozoic convergent orogenic belts in western Inner Mongolia (China): framework, kinematics, geochronology and implication for tectonic evolution of Central Asian Orogenic Belt. *Gondwana Research* **23**, 1342–64.
- Xu B and Chen B** (1997) Framework and evolution of the middle Paleozoic Orogenic Belt between Siberian and North China Plates in northern Inner Mongolia. *Science in China. Series D* **27**, 227–32 (in Chinese with English abstract).
- Xu B, Zhao GC, Li JH, Liu DX, Wang B, Han YG, Eizenhöfer PR, Zhang XR, Hou WZ and Liu Q** (2017) Ages and Hf isotopes of detrital zircons from Paleozoic strata in the Chagan Obo Temple area, Inner Mongolia: implications for the evolution of the Central Asian Orogenic Belt. *Gondwana Research* **43**, 149–63.
- Xu B, Zhao P, Bao QZ, Zhou YH, Wang YY and Luo ZW** (2014) Preliminary study on the pre-Mesozoic tectonic unit division of the Xing'an-Mongolian Orogenic Belt (XMOB). *Acta Petrologica Sinica* **30**, 1841–57 (in Chinese with English abstract).
- Xu B, Zhao P, Wang YY, Liao W, Luo ZW, Bao QZ and Zhou YS** (2015) The pre-Devonian tectonic framework of Xing'an-Mongolian Orogenic Belt (XMOB) in North China. *Journal of Asian Earth Sciences* **97**, 183–96.
- Xu G, Liu HC, Li YL, Xu Z and Xie Y** (2019) Early Permian Sonidyouqi supra-subduction-zone ophiolites in the central Solonker suture zone (Inner Mongolia, China). *Geoscience Frontiers* **10**, 1101–11.

- Xu LQ** (2005) The characteristics of magmatic rocks and discussion of geotectonics evolution from Caledonian through Hercynian to Indosinian stage in the Baiyun'ebo-Mandula Region, Inner Mongolia. PhD thesis, School of Earth Sciences and Resources, China University of Geosciences (Beijing), Beijing, China (in Chinese with English abstract). Published thesis.
- Yang JH, Wu FY, Shao JA, Wilde SA, Xie LW and Liu XM** (2006) Constraints on the timing of uplift of the Yanshan Fold and Thrust Belt, North China. *Earth and Planetary Science Letters* **246**, 336–45.
- Yang JQ** (2016) Magmatic evolution and its relationship with metallogenesis in Erenhot–Dongwuqi Area. PhD thesis, School of Earth Sciences and Resources, China University of Geosciences (Beijing), Beijing, China (in Chinese with English abstract). Published thesis.
- Yang WL, Luo MS, Wang CG and Xu ZL** (2014) Neoproterozoic–Paleozoic sedimentary basins evolution of Xing'an–Mongolian Orogenic Belt. *Earth Science: Journal of China University of Geosciences* **39**, 1155–68 (in Chinese with English abstract).
- Yang WS** (2017) The petrological and geochemical characteristics of ophiolite on the area of Diyanmiao in the Inner Mongolia. PhD thesis, Chinese Academy of Geological Sciences, Beijing, China (in Chinese with English abstract). Published thesis.
- Yang ZL, Wang SQ, Hu XJ, Xin HT and Li CD** (2018) Geochronology and geochemistry of early Paleozoic gabbroic diorites in East Ujimqin Banner of Inner Mongolia and their geological significance. *Acta Petrologica et Mineralogica* **37**, 349–65 (in Chinese with English abstract).
- Yang ZL, Wang SQ, Hu XJ, Zhao HL, Li CD, Xin HT and Sun LX** (2017) Petrogenesis of the early Paleozoic Jiergalantu Pluton in Inner Mongolia: constraints from geochronology, geochemistry and Nd–Hf isotopes. *Geological Bulletin of China* **36**, 1369–84 (in Chinese with English abstract).
- Yu JJ, Xu ZG and Xu FS** (1996) Tectonic setting of Ordovician volcanic rocks in northwestern Xiaoxing'anling Heilongjiang Province. *Acta Geoscientia Sinica* **17**, 54–64 (in Chinese with English abstract).
- Zhang CL, Zou HB, Li HK and Wang HY** (2013) Tectonic framework and evolution of the Tarim Block in NW China. *Gondwana Research* **23**, 1306–15.
- Zhang SH, Zhao Y, Song B, Hu JM, Liu SW, Yang YH, Chen FK, Liu XM and Liu J** (2009) Contrasting late Carboniferous and late Permian–middle Triassic intrusive belts from the northern margin of the North China block: geochronology, petrogenesis and tectonic implications. *Geological Society of America Bulletin* **120**, 181–200.
- Zhang W, Wu TR, Feng JC, Zheng RG and He YK** (2013) Time constraints for the closing of the Paleo-Asian Ocean in the Northern Alta Region: evidence from Wuliji granites. *Science China Earth Sciences* **56**, 153–64 (in Chinese).
- Zhang WY** (2008) Magmatic activity and metallogeny of Dong Ujimqin Banner, Inner Mongolia. PhD thesis, Chinese Academy of Geological Sciences, Beijing, China (in Chinese with English abstract). Published thesis.
- Zhang XH, Yuan LL, Xue FH, Yan X and Mao Q** (2015a) Early Permian A-type granites from central Inner Mongolia, North China: Magmatic tracer of post-collisional tectonics and oceanic crustal recycling. *Gondwana Research* **28**, 311–27.
- Zhang ZC, Li K, Li JF, Tang WH, Chen Y and Luo ZW** (2015b) Geochronology and geochemistry of the Eastern Erenhot ophiolitic complex: implications for the tectonic evolution of the Inner Mongolia–Daxinganling Orogenic Belt. *Journal of Asian Earth Sciences* **72**, 279–93.
- Zhao LG, Ran H, Zhang QH, Li CD, Wang HC, Zhang K, Xu YW and Hou KJ** (2012) Discovery of Ordovician pluton in Abaga Banner, Inner Mongolia and its geological significance. *Global Geology* **3**, 451–61 (in Chinese with English abstract).
- Zhou JB, Wang B, Wilde SA, Zhao GC, Cao JL, Zheng CQ and Zeng WS** (2015) Geochemistry and U–Pb zircon dating of the Toudaoqiao blueschists in the Great Xing'an Range, northeast China, and tectonic implications. *Journal of Asian Earth Sciences* **97**, 197–210.
- Zhou WX, Zhao XC, Fu D, Sun JJ, Li ZQ, Huang B and Ge MC** (2017) Geochronology and geochemistry of the Carboniferous Ulan Tolgoi granite complex from northern Inner Mongolia, China: Petrogenesis and tectonic implications for the Uliastai continental margin. *Geological Journal* **1**, 1–20.
- Zhou ZG, Zhang HF, Liu HL, Liu CF and Liu WC** (2009) Zircon U–Pb dating of basic intrusions in Slziwangqi area of middle Inner Mongolia, China. *Acta Petrologica Sinica* **25**, 1519–28 (in Chinese with English abstract).
- Zhu CY** (1986) Ordovician strata in the northern part of the greater and lesser Khingan Mountains northeast China. *Regional Geology of China* **4**, 349–58 (in Chinese with English abstract).
- Zhu DC, Mo XX, Wang LQ, Zhao ZD, Niu YL, Zhou CY and Yang YH** (2009) Petrogenesis of highly fractionated I-type granites in the Chayu Area of Eastern Gangdese, Tibet: constraints from zircon U–Pb geochronology, geochemistry and Sr–Nd–Hf isotopes. *Science China Earth Sciences* **39**, 833–48 (in Chinese with English abstract).
- Zhu MS, Baatar M, Miao LC, Anaad C, Zhang FC, Yang SH and Li YM** (2014) Zircon ages and geochemical compositions of the Manlay ophiolite and coeval island arc: implications for the tectonic evolution of South Mongolia. *Journal of Asian Earth Sciences* **96**, 108–22.